A bi-level distributed optimization framework to unlock flexibility in grid-connected energy storage systems and electric vehicle fleets

Fatemi, Saeid; Ketabi, Abbas; Mansouri, Seyed Amir

DOI
10.1016/j.est.2025.119107

Publication date
2025

Document Version
Final published version

Published in
Journal of Energy Storage

Journal of Energy Storage 140 (2025) 119107

Contents lists available at ScienceDirect

Journal of Energy Storage

journal homepage: www.elsevier.com/locate/est

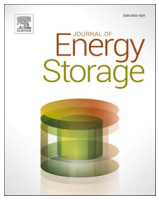

Research papers

A bi-level distributed optimization framework to unlock flexibility in grid-connected energy storage systems and electric vehicle fleets

Saeid Fatemi [a], Abbas Ketabi [a,*], Seyed Amir Mansouri [b,*]

[a] Department of Electrical and Computer Engineering, University of Kashan, 6 km Ghotbravandi Blvd, 8731753153, Kashan, Iran
[b] Department of Engineering Systems & Services, Faculty of Technology, Policy & Management, Delft University of Technology, Delft, the Netherlands

ARTICLE INFO

Keywords:
Distributed optimization
Flexibility
Virtual energy storage systems
Electric vehicle fleets
Renewable energy sources

ABSTRACT

The growing integration of renewable energy sources (RES) into power grids has introduced significant operational variability, amplifying the need for robust flexibility solutions to maintain grid reliability. Demand-side resources, such as flexible loads and electric vehicle (EV) fleets, present cost-effective avenues for balancing supply and demand dynamics. This study proposes a decentralized bi-level optimization framework to enhance the utilization of demand-side flexibility and energy storage systems while ensuring market participant privacy. A Virtual Storage Plant (VSP) model is introduced to coordinate distributed energy storage assets under the supervision of the Transmission System Operator (TSO). The upper-level problem represents the TSO's strategic planning, while the lower-level problem addresses the operation of VSPs, EV parking facilities, and flexible loads. To optimize market interactions and minimize information exchange between the TSO and service providers, an adaptive Alternating Direction Method of Multipliers (ADMM) is employed. The proposed framework is validated using a 30-bus power transmission system, solved through the GUROBI solver within the GAMS environment. The results indicate an 18.7 % reduction in energy balancing costs and a 12 % decrease in transmission losses, alongside a 60 % improvement in convergence speed, demonstrating enhanced coordination, cost efficiency, and privacy preservation.

1. Introduction

1.1. Context and motivation

The integration of RESs and EV fleets provides economic and environmental benefits but also creates operational challenges for distribution system operators, including supply–demand imbalances, voltage issues, and congestion [1–3]. To manage these challenges, renewable-based systems increasingly rely on flexible services. Prosumers with flexible loads (FLs) in smart buildings and EV parking lots can support balancing at low cost [4,5], while storage technologies such as batteries (BES), pumped hydro (PHES), and compressed air storage (CAES) offer additional flexibility [6,7]. Meanwhile, VSPs are known as interfaces that are able to control coordinated grid-connected storage systems according to the pulses received from system operators. In modern power systems, VSPs strategically manage the charging/discharging of covered storage systems to address the system's flexibility needs, thus mitigating energy production/consumption fluctuations and enhancing operational stability [8,9]. The marked rise in operational uncertainties in emerging renewable-based power systems underscores the urgency for new business models that exploit the potential of demand-side resources and VSPs [10]. These imperatives motivate this paper to propose a bi-level business model for flexibility markets, aiming to unlock the capacities of demand-side resources and VSP-supervised storage, ensure participant privacy, achieve market efficiency, and improve technical performance.

1.2. Literature review

The proliferation of RESs has intensified uncertainties in power systems, motivating extensive research on prosumer-integrated flexibility markets. In this context, [11] proposes a hierarchical model for the European balancing market, coordinating distribution and transmission networks with controllable resources such as distributed generation and EVs, achieving reduced planning costs under decentralized operation. [12] introduces a two-level Stackelberg game for cooperative transactions between distribution networks and VPPs, showing increased profits and improved cost efficiency. [13] provides a taxonomy of local

* Corresponding authors.
E-mail addresses: aketabi@kashanu.ac.ir (A. Ketabi), s.mansouri@tudelft.nl (S.A. Mansouri).

https://doi.org/10.1016/j.est.2025.119107
Received 8 July 2025; Received in revised form 22 September 2025; Accepted 20 October 2025
Available online 25 October 2025

flexibility market solutions for congestion management, offering practical recommendations based on ongoing implementations and expert input. Finally, [14] proposes a two-level model for flexible resource participation in energy, reservation, and balancing markets, showing higher profits through joint optimization of active and reactive services across grid levels.

Several studies have investigated the role of VSPs in modern power systems, underscoring their potential to deliver significant and cost-effective flexibility. [8] proposes a control approach for VSPs to manage non-programmable renewable sources by coordinating residential loads and distributed batteries, achieving peak shaving and balancing without additional compensation actions. [15] develops a two-stage VSP model using thermostatically controlled loads (TCLs), where lower-stage scheduling ensures consumer comfort based on distribution locational marginal price, and upper-stage coordination between DSO and TSO enhances system flexibility and balance. [16] analyzes merchant-owned BESs acting as VSPs in the day-ahead market, formulating the problem as a mixed-integer linear program (MILP) and extending it to a multi-VSP game. Results on the IEEE RTS-96 system show their impact on locational marginal prices and highlight differences between coordinated and competitive VSP participation.

Recent studies address flexibility and renewable uncertainty through different strategies. Demand response with telecom-based coordination reduces costs but depends on reliable communication [17], while large-scale multi-energy bases with storage and carbon capture improve long-term planning [18]. Hydrogen-based systems with fuzzy scheduling enhance operational flexibility [19], and game-theoretic models guide the deployment of charging stations for electric vehicles [20]. Integrated designs for hydrogen-ammonia production [21] and optimized hydrogen liquefaction [22] reduce costs and curtailment, while multi-timescale dispatch in solar charging stations [23] and carbon flow mapping [24] improve coordination and traceability. Further progress includes risk assessment of lightning in distribution systems [25], digitalized demand response in industrial processes [26], electric bus scheduling with charging constraints [27], and wind power error correction considering load patterns [28].

The assessment of previous research reveals that while numerous researchers have applied the ADMM to establish decentralized coordination in flexibility markets, there remains a need for enhancements to ensure rapid convergence and attainment of the global optimal solution. Several studies have utilized this algorithm for various purposes: For instance, [29] propose a decentralized ADMM-based algorithm for inter-DSO local electricity markets that preserves DSOs' privacy by exchanging limited aggregated signals, but they rely on fixed penalty parameters and do not provide adaptive penalty updates per interface or show empirical iteration savings as large as we report. [30] consider multiple TSO-DSO market models with different information sharing schemes and prove that common markets are more efficient; however, their ADMM decompositions still assume fixed coordination structures and do not exploit mixed integer storage or flexible loads jointly under changing coupling signals. In [31] the focus is on peer-to-peer energy trade and ancillary services in distribution grids, which emphasize topology and information sharing but not a full bi-level intraday balancing market with guarantee of global optimality under mixed integer constraints. [32] explicitly address uncertainty in local flexibility markets and imbalance mitigation, but their model does not jointly coordinate a VSP managing BES, PHES and CAES in combination with EV parking lots and flexible loads under adaptive penalties. Finally, [33] consider investment and distributed resource allocation for flexibility under TSO-DSO coordination, but their approach mostly centers on planning/investment horizons and less on high-resolution intraday operational market clearing with strong convergence speed improvements. In contrast, our adaptive ADMM guarantees convergence to the same global optimum as the standard ADMM, achieves significantly faster convergence, and requires only the exchange of aggregated price and quantity coupling signals, without revealing detailed states, dual variables, or internal forecasts, making it more suitable for practical intraday balancing markets with strict privacy requirements.

1.3. Research gaps

The review of existing literature highlights several important gaps:

- Fragmented resource coverage. Previous works typically consider a subset of flexible resources, such as distributed storage, EVs, or flexible loads, but do not provide a unified market mechanism that jointly integrates all of them. In particular, the joint coordination of VSP-controlled BES, PHES, and CAES, together with EV parking facilities and flexible loads, within a single intraday balancing market has not been comprehensively addressed.
- Centralized or single-layer coordination. Many studies adopt centralized clearing approaches or hierarchical structures with extensive information exchange. This raises privacy concerns and creates communication burdens that limit scalability. A fully decentralized approach with limited information sharing across independent actors remains insufficiently developed.
- Convergence limitations of standard ADMM. While ADMM has been widely applied in flexibility markets, most implementations use fixed penalty parameters, which often slow convergence or risk stalling in large-scale problems. There is a need for adaptive mechanisms that accelerate convergence without compromising optimality.
- Insufficient empirical quantification. The literature does not adequately quantify the combined technical and economic impacts of integrating multiple demand-side and storage resources into intraday balancing markets, nor does it benchmark the convergence speed of adaptive vs. standard ADMM approaches.

1.4. Contributions

This paper addresses these gaps with the following contributions:

- A comprehensive bi-level market framework. We formulate the intraday balancing market as a bi-level MIQCP, where the TSO (upper level) minimizes balancing costs, and the balancing service provider (lower level), namely VSP, maximize its profits.
- A VSP coordinating multiple technologies. The VSP jointly schedules BES, PHES, and CAES systems, aligning charge/discharge actions with TSO balancing signals, and thereby ensuring both VSP profitability and system-level cost reductions.
- An adaptive ADMM algorithm. We introduce a novel variant of ADMM where penalty coefficients are updated per coupling interface and exchange prices are iteratively adjusted. This mechanism accelerates convergence, achieving the same optimum as standard ADMM but with up to 60 % fewer iterations.
- Quantified benefits from integrated demand-side flexibility. Using a modified IEEE 30-bus system with 15-minute resolution, we demonstrate that sequentially activating VSP, flexible loads, and EV parking lots yields a total 18.7 % reduction in daily TSO balancing costs, a 12 % reduction in transmission losses, improved voltage profiles, and a 60 % faster convergence compared to standard ADMM.

Together, these contributions demonstrate that the proposed model not only advances the state of the art in decentralized market design but also provides measurable operational and economic advantages over existing studies.

2. Proposed model outline

The focus of our model is on unlocking the maximum flexible demand-side capacities, along with various storage systems, to meet the cost-effective balancing needs of renewable-based power systems. These

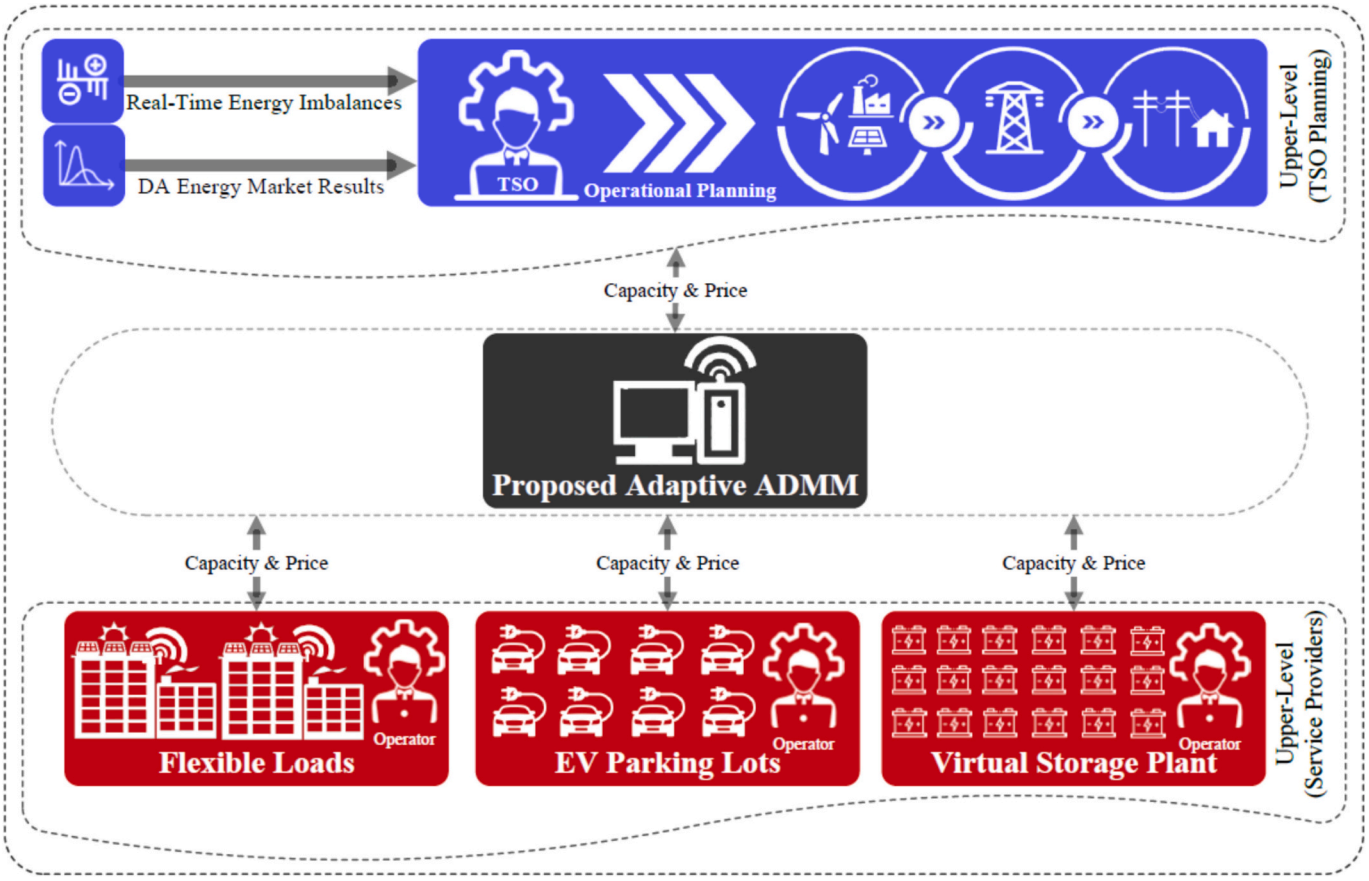

Fig. 1. The architecture of the proposed bi-level model.

needs arise from real-time changes in RESs production and system load demand. We assume that the day-ahead (DA) energy market is already settled, and its results are published. To simulate system unbalancing in the intra-day horizon, we introduce white noise using the Gaussian distribution function to the parameters related to RERs production and load demand obtained from energy market. The proposed intra-day balancing market addresses this production-consumption imbalance with a 15-minute step.

In this paper, the VSP is defined as an aggregator that jointly coordinates multiple large-scale storage technologies, namely BES, PHES, and CAES. Rather than representing a single storage unit, the VSP acts as an interface between these heterogeneous assets and the TSO, receiving aggregated balancing signals (upward/downward capacity and prices) and optimizing the charging/discharging schedules of its portfolio accordingly. This interpretation is consistent with the general role of VSPs in the literature as aggregation mechanisms, but here it is applied specifically to the coordination of large-scale storage technologies, ensuring both operational efficiency and limited information exchange with the TSO.

Fig. 1 provides an overview of the bi-level model proposed in this paper, with the TSO in the upper level and balancing service providers in the lower level. In our model, the TSO is responsible for addressing the balancing needs of its service area by utilizing the available capacities of balancing service providers, including FLs, EV parking lots, and the VSP. The TSO also controls the production planning of thermal units within the transmission network. VSP controls all storage systems connected to the grid, including BESs, PHESs, and CAESs, scheduling their charging and discharging to maximize profit from the balancing market, based on the balancing pulses received from the TSO. FLs and EV parking lots also function similarly to VSPs, maximizing profit based on pulses received from the TSO. These pulses express the required upward/downward active powers and exchange price of these services. To ensure convergence of the upper and lower levels at the global optimal point with limited information sharing, an adaptive ADMM is presented. Convergence is achieved iteratively, subject to a stopping condition. The exchange price of balancing services, defined as an input parameter in the first iteration, is updated in each iteration based on the scheduling differences of the TSO and balancing service providers. Updating this price and penalty terms, included in the objective functions of all market players, leads to convergence of the proposed adaptive ADMM.

3. Mathematical formulation

In the following, the proposed bi-level model is formulated as a Mixed-Integer Quadratic Constrained Program (MIQCP). The indices f, v, p, g, w and s refer to FL, VSP, EV parking lot, dispatchable units, wind farm and PV farm, respectively. Additionally, indices t, i and l respectively refer to time, bus, and line. Note that letters adorned with a hat symbol (ˆ) denote parameters obtained from the energy market.

3.1. Objective functions

In Eq. (a1), the upper level objective function is described, through which the TSO aims to minimize the balancing costs of the transmission system within the intraday balancing market. This function incorporates the costs paid to balancing service providers for covering energy imbalances in the transmission system. λ_f^{FL}, λ_p^{EVPL}, and λ_e^{VSP} represent the cost per megawatt of services purchased from FLs, EV parking lots, and VSP, respectively. These costs are input parameters in the initial iteration of the ADMM algorithm. In subsequent iterations, they are updated based on the ADMM penalty coefficients and the discrepancies between the upper and lower level planning outcomes. It is assumed that the

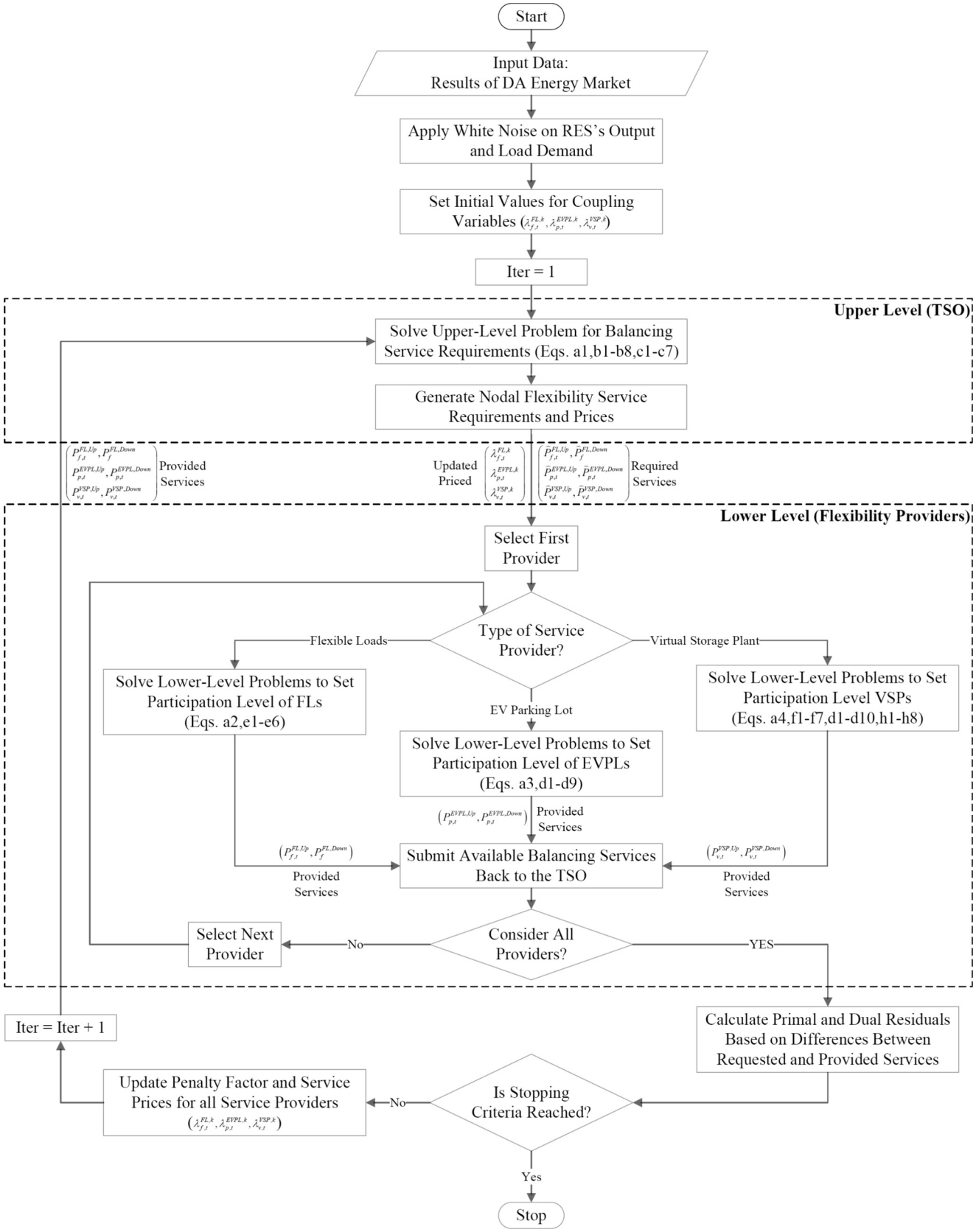

Fig. 2. The implementation of the proposed model.

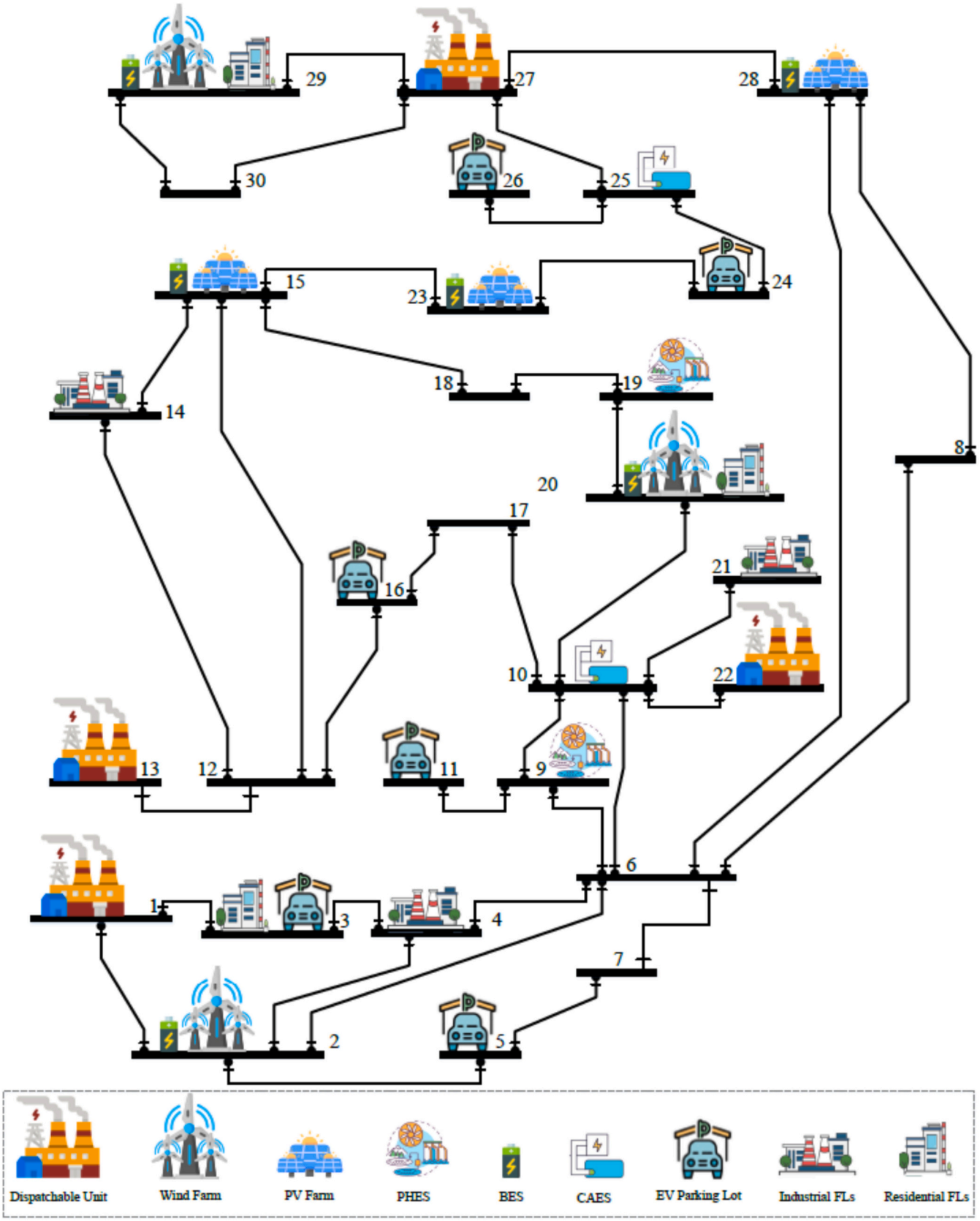

Fig. 3. Use case: Modified IEEE 30-bus test system [38].

Table 1
Specifications of case studies.

Case	Balancing service providers				Coordinator
	Dispatchable units	VSP	FLs	EV parking lots	
C1	✓	×	×	×	Proposed adaptive ADMM
C2	✓	✓	×	×	Proposed adaptive ADMM
C3	✓	✓	✓	×	Proposed adaptive ADMM
C4	✓	✓	✓	✓	Proposed adaptive ADMM
C5	✓	✓	✓	✓	Original ADMM

operating points of dispatchable units are determined in the DA energy market. If their operating points are adjusted in the intraday balancing market, the TSO compensates them accordingly. Specifically, if their operating points increase, they are compensated at the $C_g^{G,Penalty}$price, and vice versa.

$$\min OF^{TS} = \sum_t \left[\begin{array}{l} \sum_f \lambda_{f,t}^{FL}\left(P_{f,t}^{FL,Up} + P_f^{FL,Down}\right) + \sum_p \lambda_{p,t}^{EVPL}\left(P_{p,t}^{EVPL,Up} + P_{p,t}^{EVPL,Down}\right) \\ + \sum_v \lambda_{v,t}^{VSP}\left(P_{v,t}^{VSP,Up} + P_{v,t}^{VSP,Down}\right) + \sum_g C_g^{G,Penalty}\left(P_{g,t}^{G,Up} - P_{g,t}^{G,Down}\right) \end{array} \right] \Delta t \tag{a1}$$

In Eqs. (a2)–(a4), the lower level objective functions are outlined, corresponding respectively to FLs, EV parking lots, and VSP. These objective functions aim to maximize the profit of the service providers. Eq. (a2) illustrates that the FLs' objective function is modeled as the difference between revenues from providing upstream/downstream services to the market and the costs associated with load demand increases/decreases. Following a similar approach, Eq. (a3) details the objective function for EV parking lots. Eq. (a4) indicates that the profit for VSPs is calculated as the difference between revenues from offering upward/downward services to the market and the costs for charging or discharging storage systems.

$$\max OF_f^{FL} = \sum_t \left[\begin{array}{l} \sum_f \lambda_f^{FL}\left(P_{f,t}^{FL,Up} + P_{f,t}^{FL,Down}\right) \\ -\sum_f \left(C_f^{FL,Up} P_{f,t}^{FL,Up} + C_f^{FL,Down} P_{f,t}^{FL,Down}\right) \end{array} \right] \Delta t \tag{a2}$$

$$\max OF_p^{EVPL} = \sum_t \left[\begin{array}{l} \sum_p \lambda_p^{EVPL}\left(P_{p,t}^{EVPL,Up} + P_{p,t}^{EVPL,Down}\right) \\ -\sum_p \left(C_p^{EVPL,Up} P_{p,t}^{EVPL,Up} + C_p^{EVPL,Down} P_{p,t}^{EVPL,Down}\right) \end{array} \right] \Delta t \tag{a3}$$

$$\max OF_v^{VSP} = \sum_t \left[\begin{array}{l} \sum_v \lambda_v^{VSP}\left(P_{v,t}^{VSP,Up} + P_{v,t}^{VSP,Down}\right) \\ -\sum_v \left(C_v^{VSP,Up} P_{v,t}^{VSP,Up} + C_v^{VSP,Down} P_{v,t}^{VSP,Down}\right) \end{array} \right] \Delta t \tag{a4}$$

3.2. Operational constrains

3.2.1. Power flow program

Linearize AC optimal power flow (OPF) program is detailed in (b1)–(b8) [34]. Eq. (b1) expresses the relationship between the voltage characteristics of the busbars at the beginning and end of each line with active power. The corresponding relationship for reactive power is articulated in Eq. (b2). Eq. (b3) outlines the method for calculating losses, which considers the active and reactive power flowing through the lines as well as the resistance of the line. Eq. (b4) specifies the voltage magnitude limits for network buses. The voltage angle limits for grid busbars are given in Eq. (b5). Eq. (b6) caps the active and reactive power flows to line capacities. The power balance relationship for each bus is delineated in Eq. (b7), requiring that the power input to each bus equals the power output from that bus. Eq. (b8) models the balance of reactive power at each bus. Energy unbalancing is introduced into the model through a parameter generated using the Gaussian distribution function (ϖ), creating white noise on the load demand and RESs production parameters. It is noted that the proposed balancing market is held to address this energy unbalancing.

$$\frac{P_{l,t}^{Flow}}{S^{Base}} = G_l\left(V_{i,t} - V_{j,t}\right) + B_l\left(\theta_{i,t} - \theta_{j,t}\right) + \frac{P_{l,t}^{Loss}}{2} \tag{b1}$$

$$\frac{Q_{l,t}^{Flow}}{S^{Base}} = B_l\left(V_{i,t} - V_{j,t}\right) - G_l\left(\theta_{i,t} - \theta_{j,t}\right) \tag{b2}$$

$$P_{l,t}^{Loss} = \frac{R_l\left[\left(P_{l,t}^{Flow}\right)^2 + \left(Q_{l,t}^{Flow}\right)^2\right]}{S^{Base}} \tag{b3}$$

$$V^{\min} \le V_{i,t} \le V^{\max} \tag{b4}$$

$$\theta^{\min} \le \theta_{i,t} \le \theta^{\max} \tag{b5}$$

$$\left(P_{l,t}^{Flow}\right)^2 + \left(Q_{l,t}^{Flow}\right)^2 \le \left(S_l^{Flow,\max}\right)^2 \tag{b6}$$

$$\begin{aligned} &\sum_{g\in\Omega_i^g}\left(\widehat{P}_{g,t}^{G} + P_{g,t}^{G,Up} - P_{g,t}^{G,Down}\right) + \sum_{s\in\Omega_i^s}\left(\varpi_{s,t} P_{s,t}^{PV}\right) + \sum_{w\in\Omega_i^w}\left(\varpi_{w,t} P_{w,t}^{WT}\right) \\ &+ \sum_{p\in\Omega_i^p}\left(P_{p,t}^{EVPL,Up} - P_{p,t}^{EVPL,Down}\right) + \sum_{v\in\Omega_i^v}\left(P_{v,t}^{BES,Up} - P_{v,t}^{BES,Down}\right) \\ &+ \sum_{v\in\Omega_i^v}\left(P_{v,t}^{PHES,Up} - P_{v,t}^{PHES,Down}\right) + \sum_{v\in\Omega_i^v}\left(P_{v,t}^{PSU,Up} - P_{v,t}^{PSU,Down}\right) \\ &+ \sum_{v\in\Omega_i^v}\left(P_{v,t}^{CAES,Up} - P_{v,t}^{CAES,Down}\right) = \varpi_{i,t} P_{i,t}^{D}\Big|_{i\neq f} + P_{i,t}^{D}\Big|_{i=f} + \sum_{v\in\Omega_i^v} P_{v,t}^{CAES,S} + \sum_l \kappa_{i,l} P_{l,t}^{Flow} \end{aligned} \tag{b7}$$

$$\sum_{g\in\Omega_i^g} Q_{g,t}^{G} + \sum_{s\in\Omega_i^s} Q_{s,t}^{PV} + \sum_{w\in\Omega_i^w} Q_{w,t}^{WT} = \varpi_{i,t} Q_{i,t}^{D}\Big|_{i\neq f} + Q_{i,t}^{D}\Big|_{i=f} + \sum_l \kappa_{i,l} Q_{l,t}^{Flow} \tag{b8}$$

3.2.2. Generation units

Constraints related to the utilization of generation units are outlined in Eqs. (c1)–(c7). Eq. (c1) specifies the limitation on active power generation by dispatchable units. $\widehat{P}_{g,t}^{G}$ represents the generation point of dispatchable unit g in the DA energy market; $P_{g,t}^{G,Up}$ and $P_{g,t}^{G,Down}$ respectively indicate the increase and decrease in the generation point of

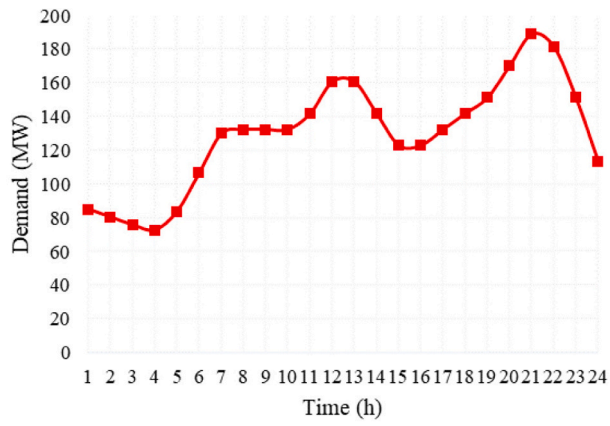

(a) Network load demand in energy market

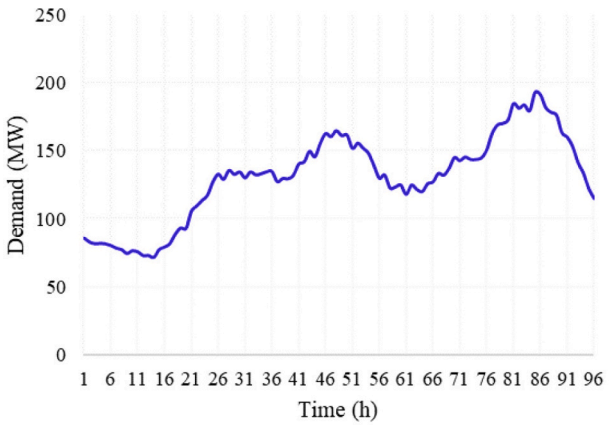

(b) Network load demand in balancing market

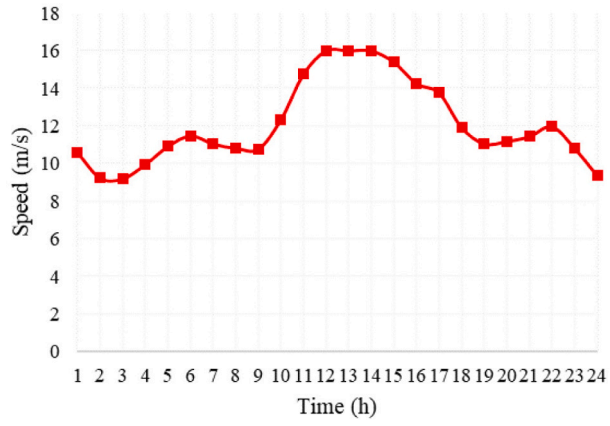

(c) Wind Speed in energy market

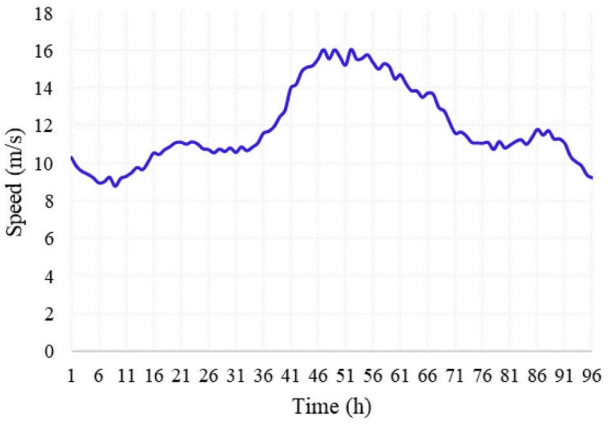

(d) Wind Speed in balancing market

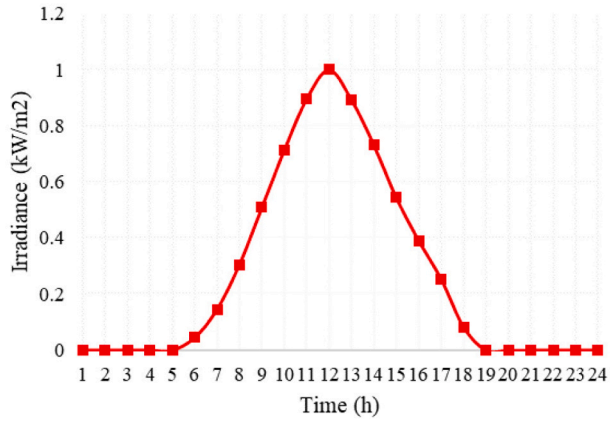

(e) Irradiance in energy market

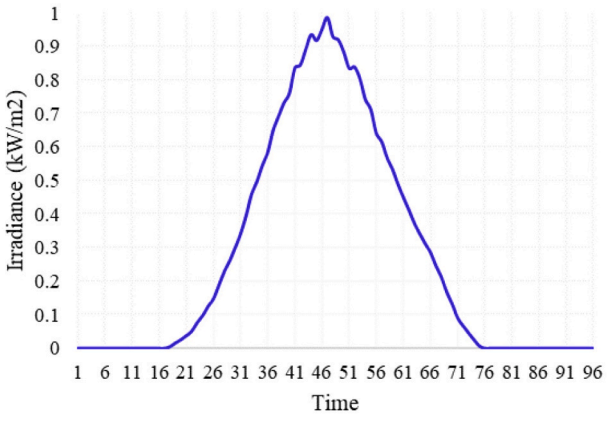

(f) Irradiance in balancing market

Fig. 4. Information on load demand, wind, and irradiance.

dispatchable unit g in the intraday balancing market. The limit on reactive power for dispatchable units is defined in Eq. (c2). In Eq. (c3), the operating point of dispatchable unit g at time t is determined based on the upward and downward services it provides. Eq. (c4) calculates the power output of solar energy per hour. Given the dependency of the reactive power of solar power plants on its active power, Eq. (c5) specifies the permissible range for injection/absorption of reactive power. Eq. (c6) determines the output active power of wind farms, considering the hourly wind speed and the technical specifications of the turbines. Eq. (c7), on the other hand, calculates the reactive power absorbed or injected by the wind farm.

$$P_g^{\min,G} \le \widehat{P}_{g,t}^{G} + P_{g,t}^{G,Up} - P_{g,t}^{G,Down} \le P_g^{\max,G} \tag{c1}$$

$$Q_g^{\min,G} \le Q_{g,t}^{G} \le Q_g^{\max,G} \tag{c2}$$

$$P_{g,t}^{G} = \widehat{P}_{g,t}^{G} + P_{g,t}^{G,Up} - P_{g,t}^{G,Down} \tag{c3}$$

$$P_{s,t}^{PV} \le \eta^{PV} \frac{R_{t,\omega}}{R^{STC}} P_s^{Rate} \tag{c4}$$

$$-\vartheta_s P_{s,t}^{PV} \le Q_{s,t}^{PV} \le \vartheta_s P_{s,st}^{PV} \tag{c5}$$

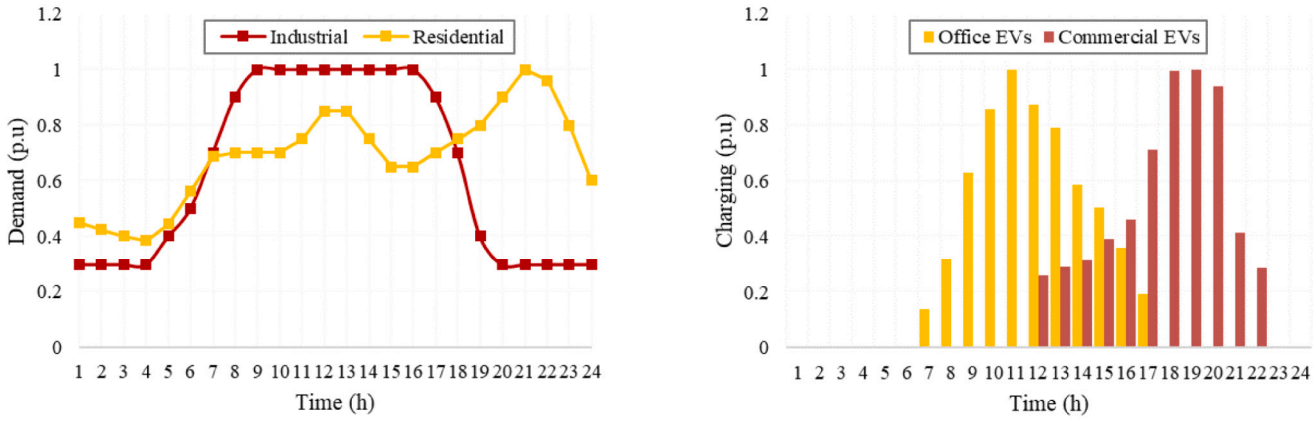

(a) FLs (b) EV parking lots

Fig. 5. Load demand of FLs and EV parking loads.

Table 2
Information on generation units, storage systems, FLs and EV parking lots.

Dispatchable units			
Number	Connected bus	Capacity (MW)	Marginal cost ($/MWh)
1	1	25	23
2	22	25	21
3	27	20	27
4	13	30	35

Renewable energy sources					
Wind farms			PV farms		
Number	Connected bus	Capacity (MW)	Number	Connected bus	Capacity (MW)
1	2	20	1	23	10
2	20	10	2	15	7
3	29	20	3	28	10

VSP-controlled energy storage systems	
Type	Connected bus
BES	2-15-20-23-28-29
PHES	9-19
CAES	10-25

EV parking lots					
Number	Connected bus	Number of EVs	Number	Connected bus	Number of EVs
1	3	400	4	16	370
2	5	500	5	24	520
3	11	400	6	26	475

Flexible loads					
Type	Connected bus	Load (MW)	Type	Connected bus	Load (MW)
Residential	3	1	Industrial	4	1.5
Residential	20	0.9	Industrial	14	1.8
Residential	29	1.1	Industrial	21	2.1

Table 3
Numerical results for case studies.

Case studies	Daily costs ($)				
	Dispatchable units	VSP	FLs	EV parking lots	Sum
C1	2132.9	–	–	–	2132.9
C2	1477.7	511.0416	–	–	1988.7416
C3	1115.8	453.744	303.0825	–	1872.6265
C4	705.6	453.5784	303.5655	270.48	1733.2239
C5	705.6	453.5784	303.5655	270.48	1733.2239

$$P_{w,t}^{WT} \le \begin{cases} 0 & , \quad V_{t,\omega} < V_w^{ci} \ \ or \ \ V_t \ge V_w^{co} \\ P_w^{Rate} \dfrac{V_t - V_w^r}{V_w^{ci} - V_w^r} & , \quad V_w^{ci} \le V_t < V_w^r \\ P_w^{Rate} & , \quad V_w^r \le V_t < V_w^{co} \end{cases} \tag{c6}$$

$$-\vartheta_w P_{w,t}^{WT} \le Q_{w,t}^{WT} \le \vartheta_w P_{w,t}^{WT} \tag{c7}$$

3.2.3. EV parking lots

In Eqs. (d1)–(d9) the restrictions related to the parking of EVs are presented [2]. In Eq. (d1), the initial charge of EVs is determined using the normal distribution function with mean μ and variance σ. In Eq. (d2), the charge level in the battery of EVs is determined every hour. This charge level is a function of the charge level of the previous hour ($SoC_{ev,t-1}$) and charge ($P_{ev,t}^{Ch}$) or discharge ($P_{ev,t}^{Dis}$) in the current hour. The maximum hourly charge and discharge limits are provided in Eqs. (d3) and (d4), respectively. The level of energy that can be stored in the EV battery is limited in Eq. (d5). It is stated in Eq. (d6) that the level of energy stored in the car when the EV leaves the parking lot must be within the predetermined allowed range. This value for energy and density markets is set equal to the average of the two minimum ($SoC_{ev}^{Departure,\min}$) and maximum ($SoC_{ev}^{Departure,\max}$) charging levels. In order to prevent simultaneous charging and discharging of the vehicle, the limit given in Eq. (d7) has been used. Considering that EV parking can participate in the balancing market, in Eq. (d8) their participation amount for flexibility services is calculated according to the change of their charge and discharge amount. It is assumed that each parking lot has a preferred schedule for charging ($\widehat{P}_{ev,t}^{Ch}$) and discharging ($\widehat{P}_{ev,t}^{Dis}$) its covered vehicles, which it needs to change in order to participate in the balancing market. Finally, in Eq. (d9), the reactive power injection/

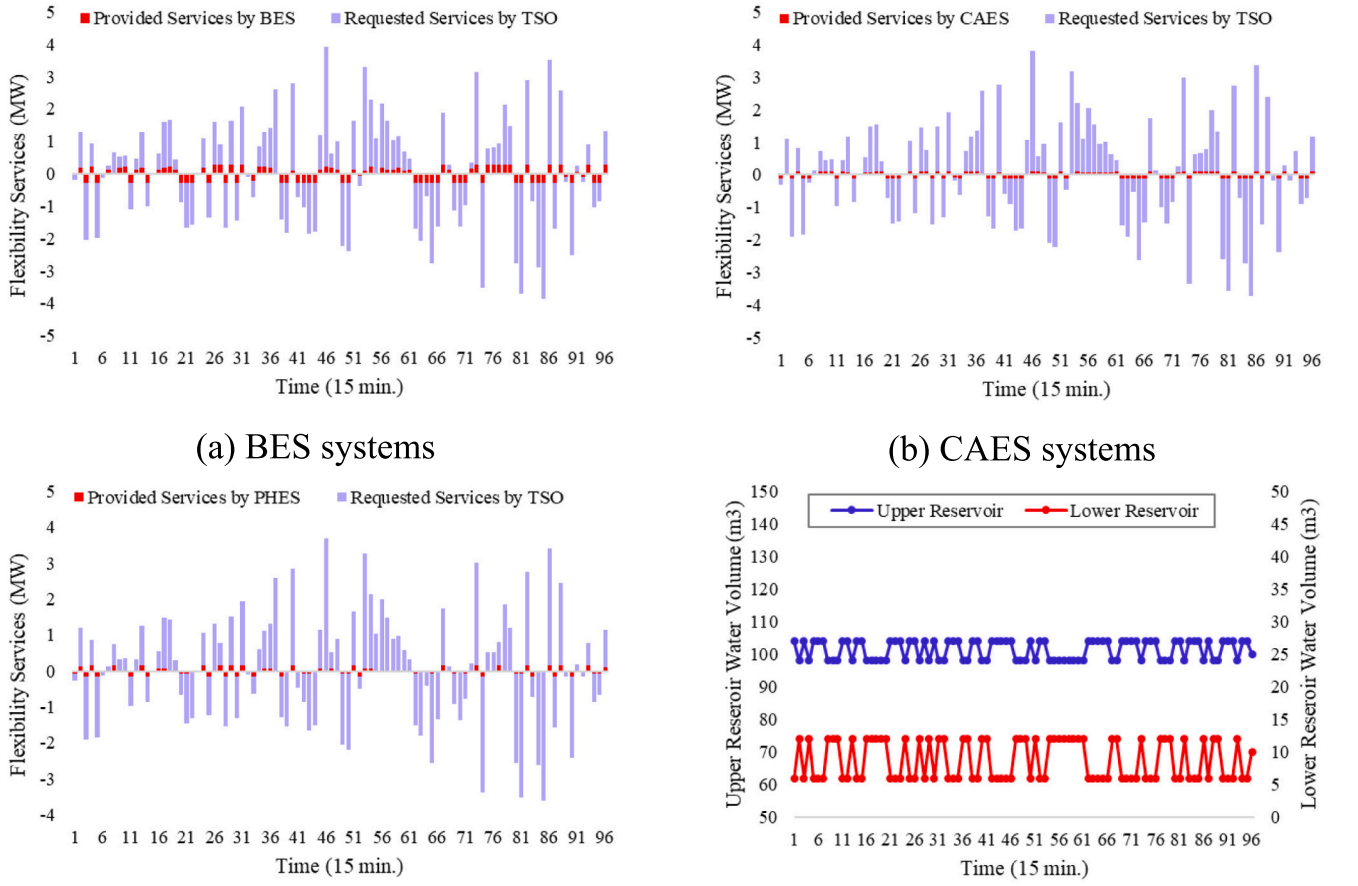

Fig. 6. Operational Scheduling of energy storage systems.

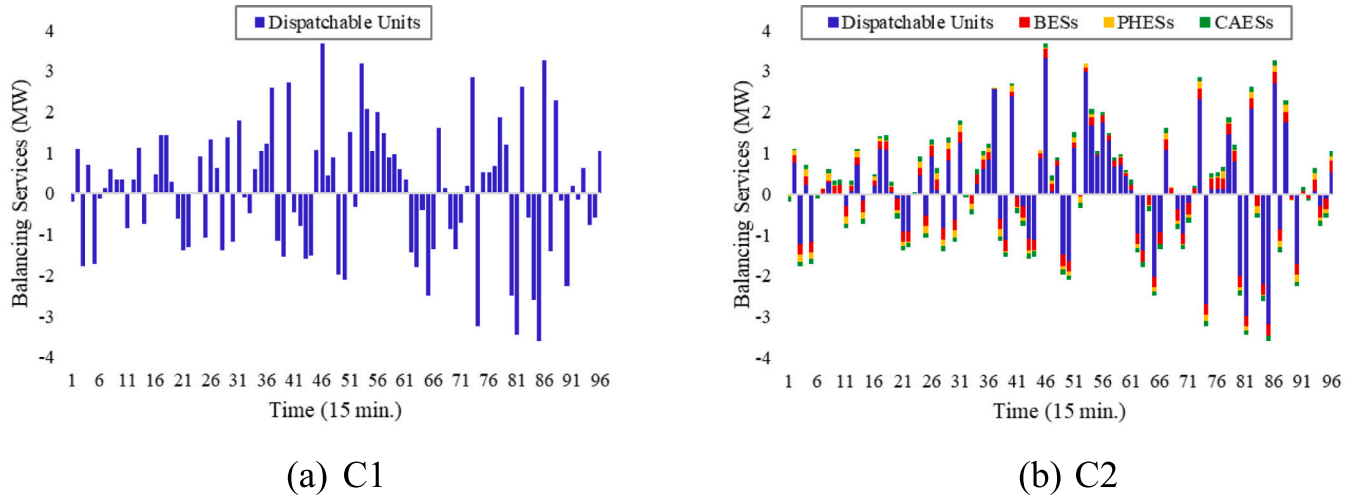

Fig. 7. Balancing service providers.

absorption limit by parking chargers is determined according to the active power consumption.

$$SoC_{ev,t=Arrival} = F_{Gaussian}\left(\mu, \sigma^2\right) \tag{d1}$$

$$SoC_{ev,t} = SoC_{ev,t-1} + \left(P^{Ch}_{ev,t}\eta^{Ch} - \frac{P^{Dis}_{ev,t}}{\eta^{Dis}}\right)\Delta t \tag{d2}$$

$$0 \le P^{Ch}_{ev,t} \le P^{Ch,\max}_{ev,t} I^{Ch}_{ev,t} \tag{d3}$$

$$0 \le P^{Dis}_{ev,t} \le P^{Dis,\max}_{ev,t} I^{Dis}_{ev,t} \tag{d4}$$

$$SoC^{\min}_{ev} \le SoC_{ev,t} \le SoC^{\max}_{ev} \tag{d5}$$

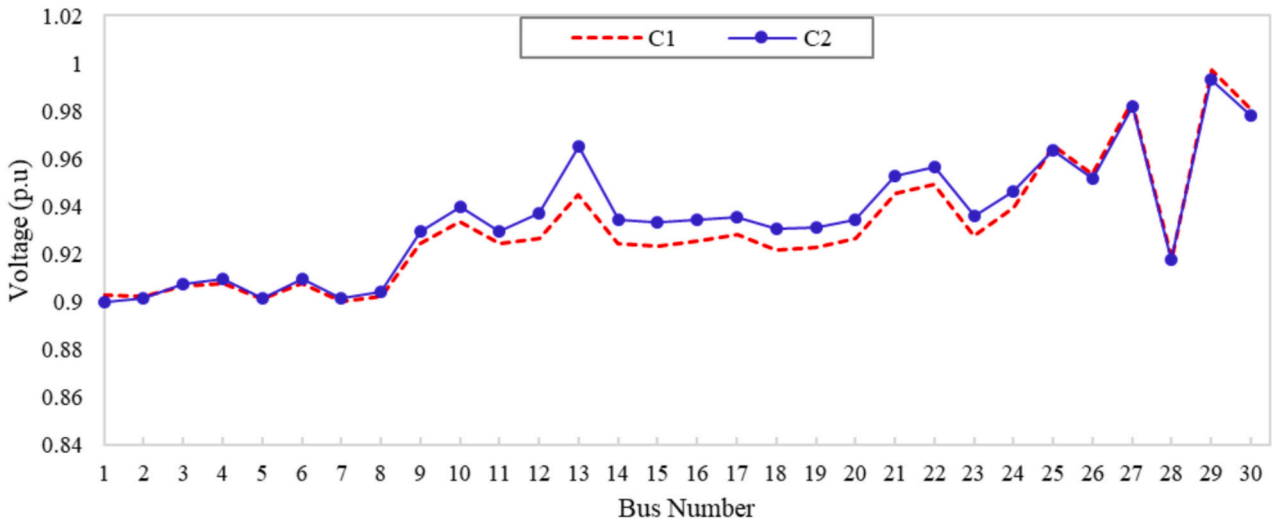

Fig. 8. Voltage profile at 21:45 in C1 & C2.

$$SoC_{ev}^{Departure,\min} \le SoC_{ev,t=Departure} \le SoC_{ev}^{Departure,\max} \tag{d6}$$

$$I_{ev,t}^{Ch} + I_{ev,t}^{Dis} \le 1 \tag{d7}$$

$$P_{p,t}^{EVPL,Down} - P_{p,t}^{EVPL,Up} = \sum_{ev\in\Omega_p^{ev}} \left(P_{ev,t}^{Ch} - \widehat{P}_{ev,t}^{Ch} \right) + \sum_{ev\in\Omega_p^{ev}} \left(\widehat{P}_{ev,t}^{Dis} - P_{ev,t}^{Dis} \right) \tag{d8}$$

$$\left(P_{p,t}^{EVPL,Down} + P_{p,t}^{EVPL,Up} \right)^2 + \left(Q_{p,t}^{EVPL} \right)^2 \le \left(S_p^{EVPL,Charger} \right)^2 \tag{d9}$$

3.2.4. Flexible loads

In Eqs. (e1)–(e6), the constraints related to flexible industrial/residential loads are detailed. Eq. (e1) specifies the amount of active load consumed at flexible points, including their participation in the balancing market ($P_{i,t,\omega}^{Up,D}/P_{i,t,\omega}^{Down,D}$). Eqs. (e2) and (e3) establish the maximum allowable participation for reducing or increasing the load, respectively. To prevent the simultaneous increase and decrease of load, Eq. (e4) is introduced. Eq. (e5) prevents the load shedding in FLs. Finally, Eq. (e6) computes the variations in reactive power at flexible points, based on changes in active power.

$$P_{i,t,\omega}^{D} = P_{i,t,\omega}^{Load} - P_{i,t}^{Up,D} + P_{i,t}^{Down,D} \tag{e1}$$

$$0 \le P_{i,t}^{Up,D} \le \alpha_i^{Up} P_{i,t}^{Load} I_{i,t}^{Up} \tag{e2}$$

$$0 \le P_{i,t}^{Down,D} \le \alpha_i^{Down} P_{i,t}^{Load} I_{i,t}^{Down} \tag{e3}$$

$$I_{i,t}^{Up} + I_{i,t}^{Down} \le 1 \tag{e4}$$

$$\sum_t P_{i,t}^{Up,D} \Delta t = \sum_t P_{i,t}^{Down,D} \Delta t \tag{e5}$$

$$Q_{i,t,\omega}^{D} = Q_{i,t,\omega}^{Load} \frac{P_{i,t}^{D}}{P_{i,t}^{Load}} \tag{e6}$$

3.2.5. Virtual storage plant

Energy storage systems under VSP control, including BESs, PHESs, and CAESs, are modeled in Eqs. (f1)–(h8). The operation of BES is detailed in Eqs. (f1)–(f7). Eq. (f1) calculates the energy stored in the battery each hour, based on the hourly charge and discharge activities by the end of each hour. Eq. (f2) establishes the hourly charging limit, while the hourly discharge limit is defined in Eq. (f3). Eq. (e4) prohibits simultaneous charging and discharging of the BES. Eq. (f5) delineates the BES's capacity limit. Eq. (f6) guarantees that the energy level at the conclusion of the scheduling period is equal to or exceeds the initial energy level of the BES. Finally, Eq. (f7) specifies the initial energy level in the BES.

$$E_{v,t}^{BES} = E_{v,t-1}^{BES} + \left(P_{v,t}^{BES,Down} \eta^{Ch} - \frac{P_{v,t}^{BES,Up}}{\eta^{Dis}} \right) \Delta t \tag{f1}$$

$$0 \le P_{v,t}^{BES,Down} \le P_v^{BES,Ch,\max} I_{v,t}^{BES,Ch} \tag{f2}$$

$$0 \le P_{v,t}^{BES,Up} \le P_v^{BES,Dis,\max} I_{v,t}^{BES,Dis} \tag{f3}$$

$$I_{v,t}^{BES,Ch} + I_{v,t}^{BES,Dis} \le 1 \tag{f4}$$

$$E_v^{BES,\min} \le E_{v,t}^{BES} \le E_v^{BES,\max} \tag{f5}$$

$$E_{v,t=T} \ge E_v^{In,BES} \tag{f6}$$

$$E_{v,t=0} = E_v^{In,BES} \tag{f7}$$

Eqs. (g1)–(g10) describe the operational dynamics and constraints for PHES [35]. Eqs. (g1) and (g2) calculate the upper and lower energy levels of PHES at time t, factoring in the energy generated ($P_{v,t}^{PHES,Up}$) and consumed ($P_{v,t}^{PHES,Down}$) for pumping and generation, adjusted by their respective efficiency (γ^{Gen} and γ^{Pump}), over the time increment Δt. Constraints (g3) and (g4) ensure these energy levels stay within predefined upper and lower bounds. Eqs. (g5) and (g6) set the maximum pumping and generation activities based on the system's operational limits and indicator functions ($I_{v,t}^{Pump}$ and $I_{v,t}^{Gen}$), ensuring activities do not exceed maximum capacities. Constraint (g7) prevents simultaneous generation and pumping. Eqs. (g8) to (g10) establish initial and final conditions for energy levels, ensuring the final upper energy level is at least equal to the initial input and defining initial upper and lower energy levels at the start of the period.

$$V_{v,t}^{Up} = V_{v,t-1}^{Up} + \left(P_{v,t}^{PHES,Down} \gamma^{Pump} - P_{v,t}^{PHES,Up} \gamma^{Gen} \right) \Delta t \tag{g1}$$

$$V_{v,t}^{Down} = V_{v,t-1}^{Down} + \left(P_{v,t}^{PHES,Up} \gamma^{Gen} - P_{v,t}^{PHES,Down} \gamma^{Pump} \right) \Delta t \tag{g2}$$

$$V_v^{Up,\min} \le V_{v,t}^{Up} \le V_v^{Up,\max} \tag{g3}$$

$$V_v^{Down,\min} \le V_{v,t}^{Down} \le V_v^{Down,\max} \tag{g4}$$

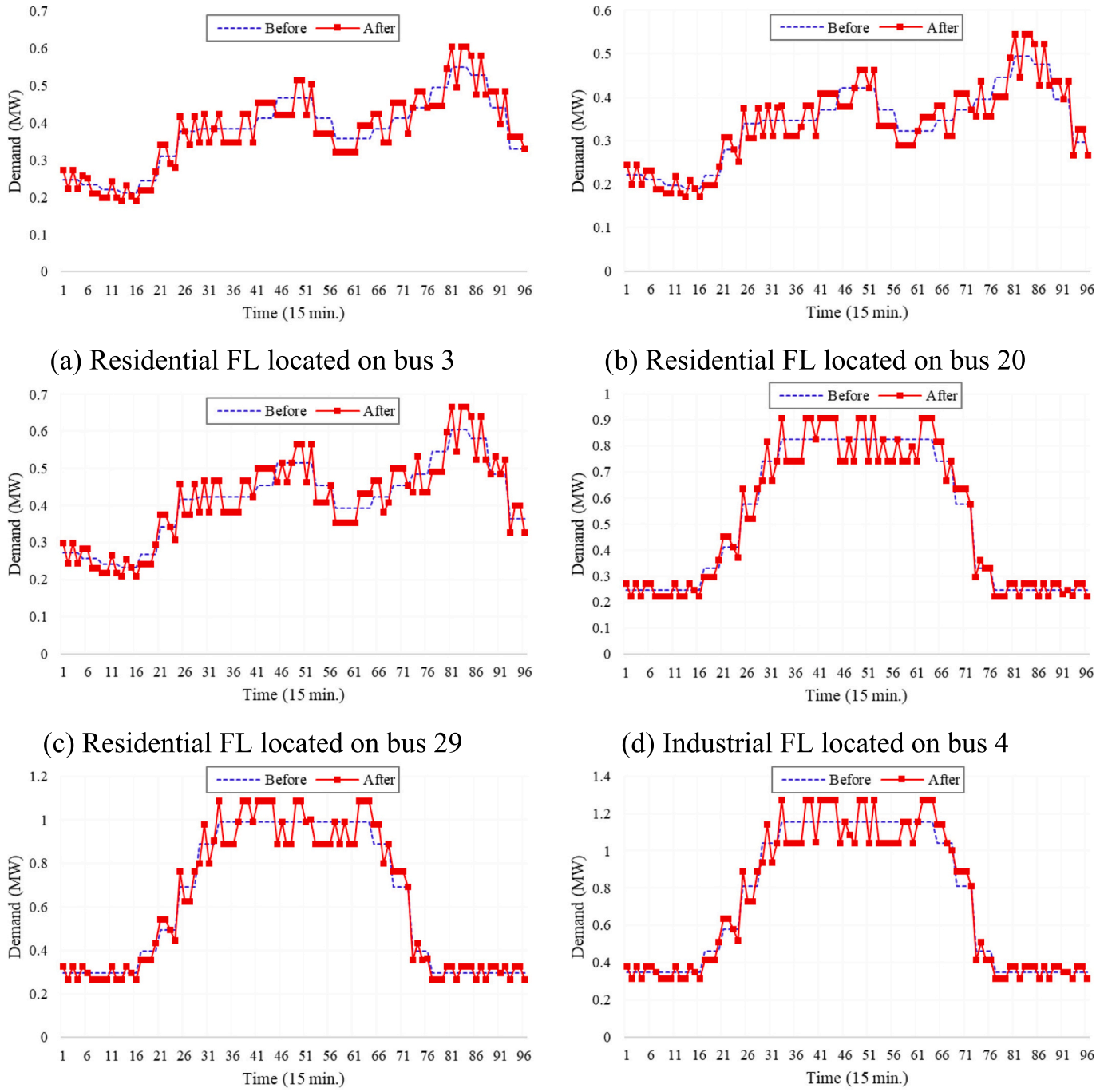

Fig. 9. Load demand curve of FLs.

$$0 \le P_{v,t}^{PHES,Down} \le P_{v}^{Pump,\max} I_{v,t}^{Pump} \quad \text{(g5)}$$

$$0 \le P_{v,t}^{PHES,Up} \le P_{v}^{Gen,\max} I_{v,t}^{Gen} \quad \text{(g6)}$$

$$I_{v,t}^{Gen} + I_{v,t}^{Pump} \le 1 \quad \text{(g7)}$$

$$V_{v,t=T}^{Up} \ge V_{v}^{In} \quad \text{(g8)}$$

$$V_{v,t=0}^{Up} = V_{v}^{In,Up} \quad \text{(g9)}$$

$$V_{v,t=0}^{Down} = V_{v}^{In,Down} \quad \text{(g10)}$$

The operation of the CAES is detailed in Eqs. (h1)–(h8) [36]. Eqs. (h1) and (h2) define the charging and discharging limits of the system, respectively. The energy stored within the CAES is computed using Eq. (h3). Eq. (h4) computes the power required to maintain the pressure in the system's tank. The allowable range of capacity for storage in the tank is specified in Eq. (h5). Eq. (h6) stipulates that the storage system operates exclusively in either charging or discharging mode at any given time. Eq. (h7) ensures that the pressure in the tank at the end of the planning period is equal or greater than the initial pressure. Lastly, Eq.

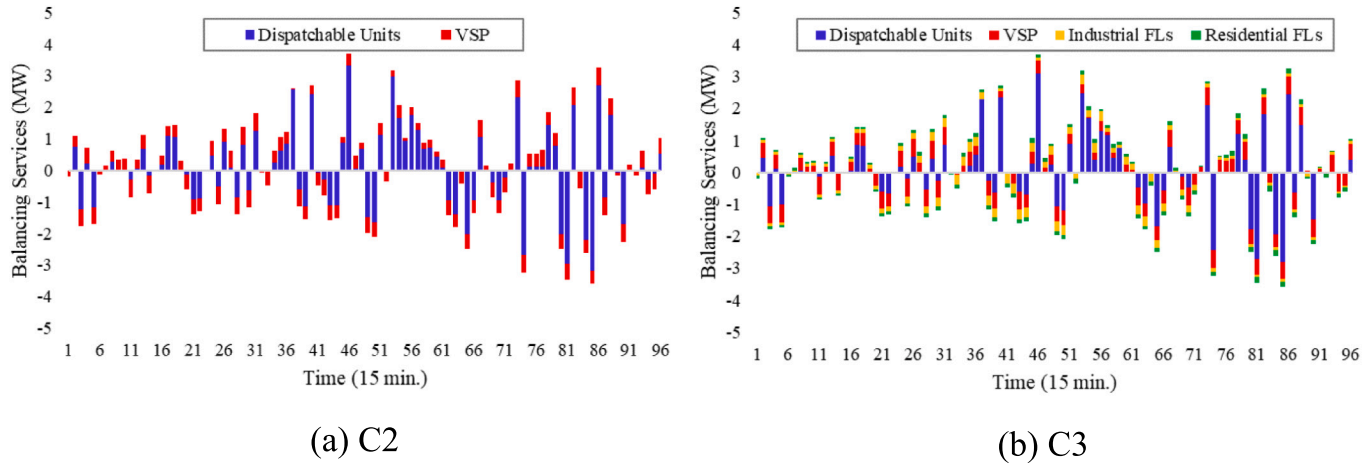

Fig. 10. Balancing service providers.

(h8) sets the initial pressure of the tank.

$$0 \le P_{v,t}^{CAES,Down} \le P_{v}^{CAES,Ch,\max} I_{v,t}^{CAES,Ch} \tag{h1}$$

$$0 \le P_{v,t}^{CAES,Up} \le P_{v}^{CAES,Dis,\max} I_{v,t}^{CAES,Dis} \tag{h2}$$

$$E_{v,t}^{CAES} = E_{v,t-1}^{CAES} + \left(P_{v,t}^{CAES,Down}\gamma^{Ch} - P_{v,t}^{CAES,Up}\gamma^{Dis}\right)\Delta t \tag{h3}$$

$$P_{v,t}^{CAES,S} = \frac{E_{v,t}^{CAES} + E_{v,t-1}^{CAES}}{2}\gamma^{S} \tag{h4}$$

$$E_{v}^{CAES,\min} \le E_{v,t}^{CAES} \le E_{v}^{CAES,\max} \tag{h5}$$

$$I_{v,t}^{CAES,Ch} + I_{v,t}^{CAES,Dis} \le 1 \tag{h6}$$

$$E_{v,t=T}^{CAES} \ge E_{v}^{In,CAES} \tag{h7}$$

$$E_{v,t=0}^{CAES} = E_{v}^{In,CAES} \tag{h8}$$

3.3. Convergence process using the proposed adaptive ADMM

The proposed adaptive ADMM algorithm is described in Eqs. (i1)–(i16). In Eqs. (i1)–(i3), the quadratic penalty terms related to service providers are detailed. These terms should be incorporated into the objective functions of FLs, EV parking lots, and VSP, respectively. Additionally, all three of these penalty terms should be included in the TSO's objective function. Incorporating these penalty terms into the objective functions at both the upper and lower levels fosters convergence of their respective programs. The penalty terms are formulated based on the discrepancy between the schedule requested by the transmission network and the final contribution from each source. During each iteration of the proposed ADMM, the coefficients pertaining to each service provider ($\varphi^{FL}/\varphi^{EVPL}/\varphi^{VSP}$) are updated individually. It is important to note that, unlike in the original ADMM method where this coefficient remains constant, in the proposed adaptive version, it is dynamically updated [37].

$$Pen^{FL} = \frac{\varphi^{FL}}{2}\left\| P_{f,t}^{FL,Up} - \widehat{P}_{f,t}^{FL,Up} + \widehat{P}_{f}^{FL,Down} - P_{f}^{FL,Down} \right\|_2^2 \tag{i1}$$

$$Pen^{EVPL} = \frac{\varphi^{EVPL}}{2}\left\| P_{p,t}^{EVPL,Up} - \widehat{P}_{p,t}^{EVPL,Up} + \widehat{P}_{p,t}^{EVPL,Down} - P_{p,t}^{EVPL,Down} \right\|_2^2 \tag{i2}$$

$$Pen^{VSP} = \frac{\varphi^{VSP}}{2}\left\| P_{v,t}^{VSP,Up} - \widehat{P}_{v,t}^{VSP,Up} + \widehat{P}_{v,t}^{VSP,Down} - P_{v,t}^{VSP,Down} \right\|_2^2 \tag{i3}$$

In Eqs. (i4)–(i9), primal ($R_{Primal}^{FL}/R_{Primal}^{EVPL}/R_{Primal}^{VSP}$) and dual residuals ($R_{Dual}^{FL}/R_{Dual}^{EVPL}/R_{Dual}^{VSP}$) are calculated based on the discrepancies between the upper and lower levels. According to these equations, it is evident that the value of the primal residuals is determined by the disparity between the services requested by the TSO and those provided by the service provider. Meanwhile, the residual value of the dual problem is derived from the variation in the exchange price of services across two consecutive iterations of the algorithm.

$$R_{Primal}^{FL} = \left\| P_{f,t}^{FL,Up} - \widehat{P}_{f,t}^{FL,Up} + \widehat{P}_{f}^{FL,Down} - P_{f}^{FL,Down} \right\|_2 \tag{i4}$$

$$R_{Dual}^{FL} = \left\| \lambda_{f,t}^{FL,k} - \lambda_{f,t}^{FL,k-1} \right\|_2 \tag{i5}$$

$$R_{Primal}^{EVPL} = \left\| P_{p,t}^{EVPL,Up} - \widehat{P}_{p,t}^{EVPL,Up} + \widehat{P}_{p,t}^{EVPL,Down} - P_{p,t}^{EVPL,Down} \right\|_2 \tag{i6}$$

$$R_{Dual}^{EVPL} = \left\| \lambda_{p,t}^{EVPL,k} - \lambda_{p,t}^{EVPL,k-1} \right\|_2 \tag{i7}$$

$$R_{Primal}^{VSP} = \left\| P_{v,t}^{VSP,Up} - \widehat{P}_{v,t}^{VSP,Up} + \widehat{P}_{v,t}^{VSP,Down} - P_{v,t}^{VSP,Down} \right\|_2 \tag{i8}$$

$$R_{Dual}^{VSP} = \left\| \lambda_{v,t}^{VSP,k} - \lambda_{v,t}^{VSP,k-1} \right\|_2 \tag{i9}$$

In Eqs. (i10)–(i12), the exchange price of balancing services at coupling points between the TSO and service providers is updated. Meanwhile, Eqs. (i13)–(i15) are responsible for updating the penalty coefficients of the proposed adaptive ADMM based on the differences between primal and dual residuals. This updating mechanism enhances the convergence speed of the proposed adaptive ADMM, thereby reducing the solution time. Eqs. (i13)–(i15) specify that if the primal residual is significantly larger than the dual residual, then the penalty coefficient increases. Conversely, if the dual residual is significantly larger than the primal residual, then the penalty coefficient decreases. Additionally, if the difference between the primal and dual residuals is not substantial, the penalty coefficient remains unchanged. The stopping criterion is presented in Eq. (i16), based on which the algorithm stops if the sum of primal and dual residuals is equal to or less than Φ. Φis assumed to be $2e^{-6}$.

$$\lambda_{f,t}^{FL,k} = \lambda_{f,t}^{FL,k-1} + \varphi^{FL,k}\left(P_{f,t}^{FL,Up} - \widehat{P}_{f,t}^{FL,Up} + \widehat{P}_{f}^{FL,Down} - P_{f}^{FL,Down}\right) \tag{i10}$$

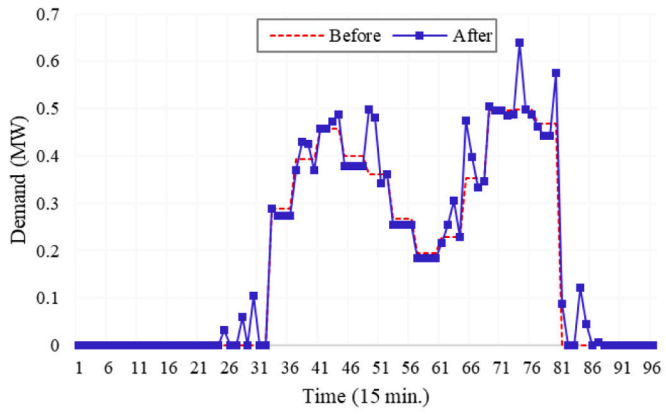

(a) EV parking lot located on bus 3

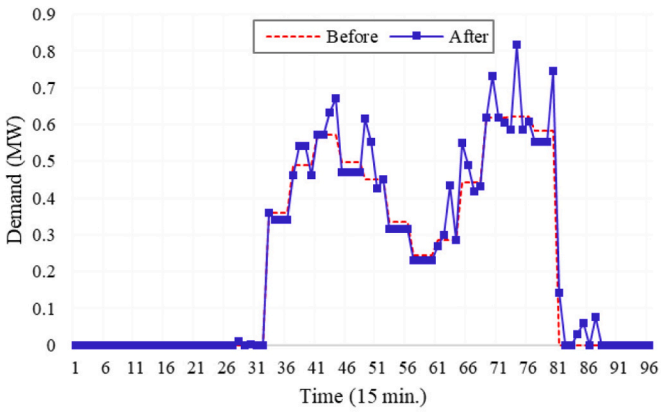

(b) EV parking lot located on bus 5

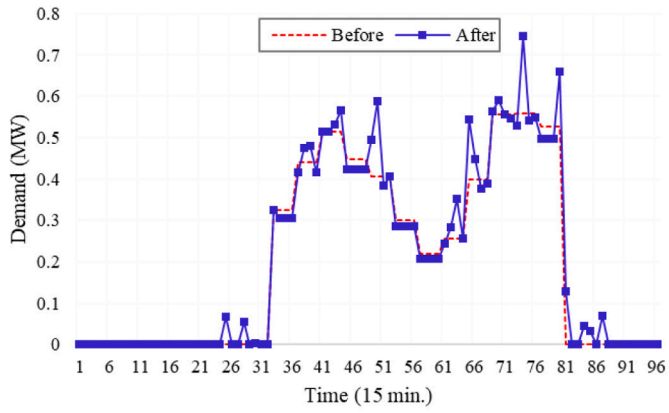

(c) EV parking lot located on bus11

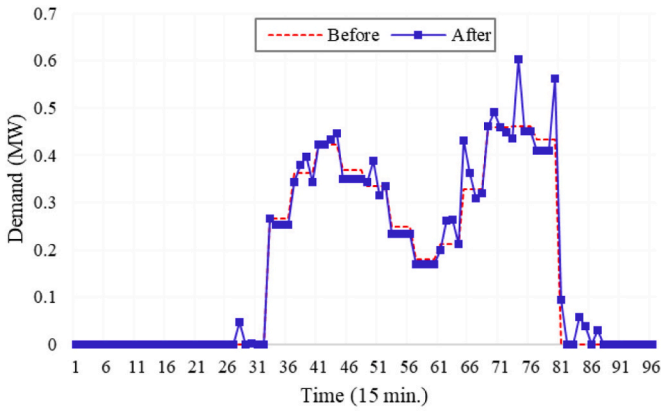

(d) EV parking lot located on bus 16

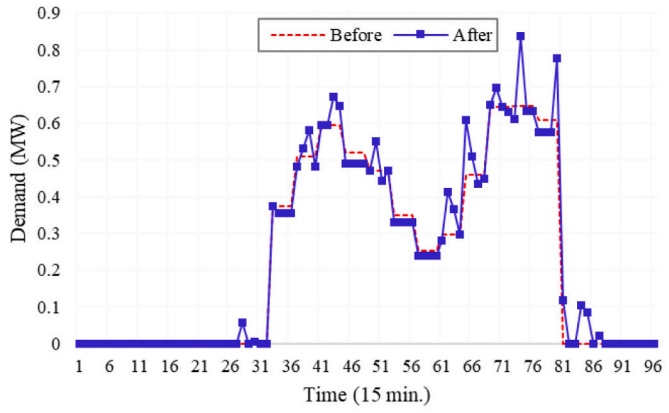

(e) EV parking lot located on bus 24

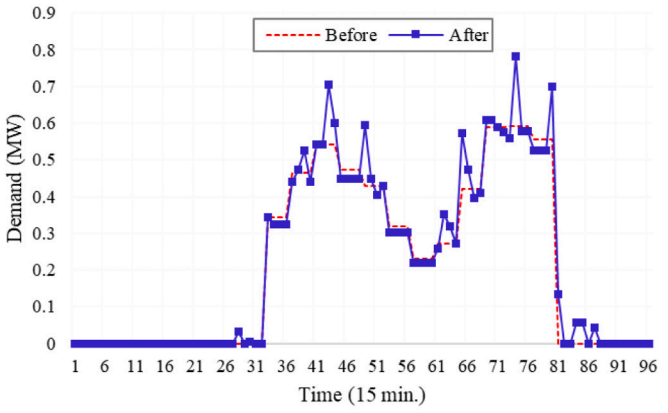

(f) EV parking lot located on bus 26

Fig. 11. EV parking lots program.

$$\lambda_{p,t}^{EVPL,k} = \lambda_{p,t}^{EVPL,k-1} + \varphi^{EVPL,k}\left(P_{p,t}^{EVPL,Up} - \widehat{P}_{p,t}^{EVPL,Up} + \widehat{P}_{p,t}^{EVPL,Down} - P_{p,t}^{EVPL,Down}\right) \tag{i11}$$

$$\lambda_{v,t}^{VSP,k} = \lambda_{v,t}^{VSP,k-1} + \varphi^{VSP,k}\left(P_{v,t}^{VSP,Up} - \widehat{P}_{v,t}^{VSP,Up} + \widehat{P}_{v,t}^{VSP,Down} - P_{v,t}^{VSP,Down}\right) \tag{i12}$$

$$\begin{cases} \varphi^{FL,k+1} = \varphi^{FL,k} \times \beta \quad , \quad R_{Primal}^{FL} >> R_{Dual}^{FL} \\ \varphi^{FL,k+1} = \varphi^{FL,k} / \beta \quad , \quad R_{Dual}^{FL} >> R_{Primal}^{FL} \\ \varphi^{FL,k+1} = \varphi^{FL,k} \quad , \quad Otherwise \end{cases} \tag{i13}$$

$$\begin{cases} \varphi^{EVPL,k+1} = \varphi^{EVPL,k} \times \beta \quad , \quad R_{Primal}^{EVPL} >> R_{Dual}^{EVPL} \\ \varphi^{EVPL,k+1} = \varphi^{EVPL,k} / \beta \quad , \quad R_{Dual}^{EVPL} >> R_{Primal}^{EVPL} \\ \varphi^{EVPL,k+1} = \varphi^{EVPL,k} \quad , \quad Otherwise \end{cases} \tag{i14}$$

$$\begin{cases} \varphi^{VSP,k+1} = \varphi^{VSP,k} \times \beta \quad , \quad R_{Primal}^{VSP} >> R_{Dual}^{VSP} \\ \varphi^{VSP,k+1} = \varphi^{VSP,k} / \beta \quad , \quad R_{Dual}^{VSP} >> R_{Primal}^{VSP} \\ \varphi^{VSP,k+1} = \varphi^{VSP,k} \quad , \quad Otherwise \end{cases} \tag{i15}$$

$$R_{Primal}^{FL} + R_{Dual}^{FL} + R_{Primal}^{EVPL} + R_{Dual}^{EVPL} + R_{Primal}^{VSP} + R_{Dual}^{VSP} \leq \Phi \tag{i16}$$

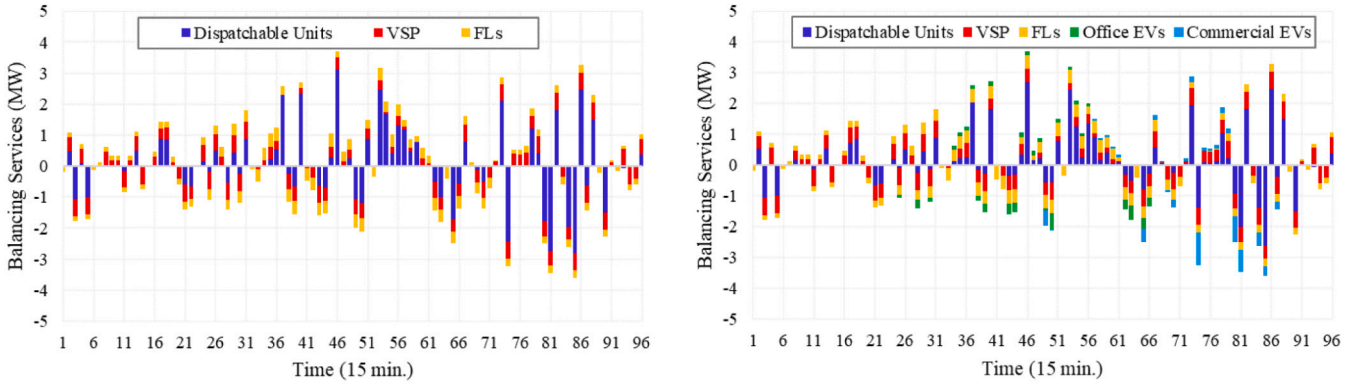

Fig. 12. Balancing service providers.

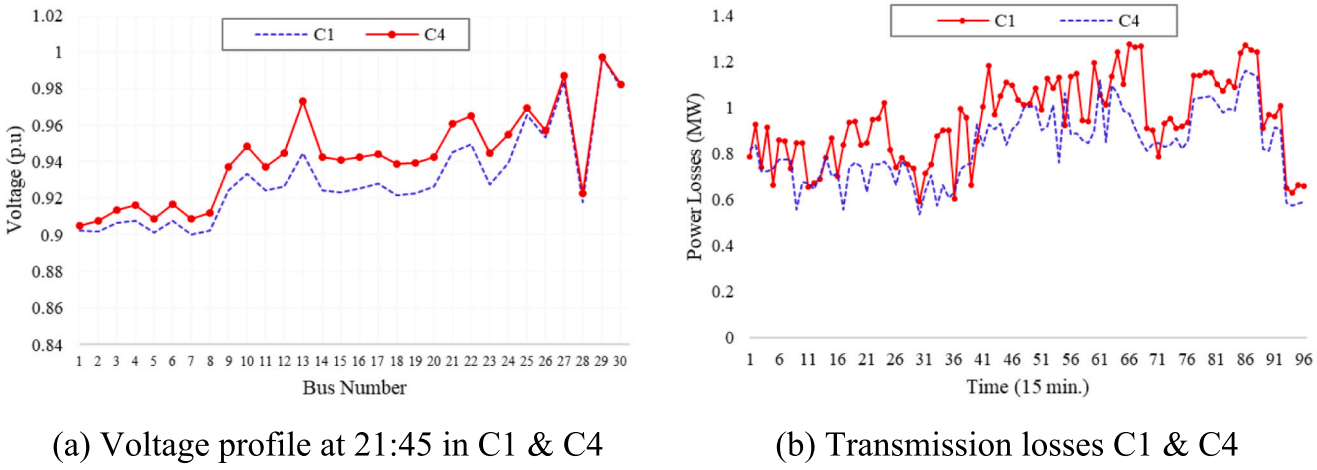

Fig. 13. Voltage profile and transmission losses.

Relation to adaptive ADMM literature. Unlike global adaptive schemes that tune a single penalty parameter from aggregate residual ratios, the proposed mechanism performs interface-specific penalty updates for each market coupling (TSO-VSP, TSO-EV, TSO-FL) and co-updates the exchange price at every iteration. This joint penalty-price update embeds the market's economic signal directly into the dual step, improving stability when coordinating heterogeneous actors (storage portfolios, EV parking, and flexible loads) within the bi-level intraday balancing formulation. Importantly, the algorithm operates with privacy-preserving aggregated signals (price/quantity) only, yet converges to the same centralized optimum under our modeling assumptions. This combination, per-interface adaptation, dual updates aligned with market prices, and operation under strict information-sharing limits, distinguishes our approach from existing adaptive ADMM variants.

4. Solution method

A flowchart presented in Fig. 2 illustrates the implementation process of the proposed adaptive ADMM-enabled bi-level model. In the first step, the day-ahead market results (generation schedules, load forecasts, and network data) are provided to the GAMS environment as initial inputs. In the second step, Gaussian white noise is applied to the RES production parameters and load demand to reflect forecast errors and create imbalances that must be addressed in the intraday balancing market. The third step initializes the coupling variables (denoted as $\lambda_{f,t}^{FL,k}$, $\lambda_{p,t}^{EVPL,k}$ and $\lambda_{v,t}^{VSP,k}$), which represent the exchanged quantities and prices between the TSO and the service providers (VSP, EV parking, and FLs). These variables are updated iteratively following the rules of the proposed adaptive ADMM (Eqs. (i10)–(i12)). In the fourth step, the upper-level problem is solved by the TSO to determine the required upward and downward balancing capacities at the coupling nodes. These requirements are then communicated to the service providers as aggregated balancing signals. In the fifth step, each service provider (VSP, EV, FL) solves its local optimization problem, considering the TSO's requested capacities, its own technical and operational constraints, and expected profits. The providers then submit their available balancing services back to the TSO. In the sixth step, the primal and dual residuals are calculated at each coupling node, reflecting the difference between the TSO's required capacities and the service providers' offered schedules. In the seventh step, the stopping criterion is checked: if the residuals are within tolerance (Φ), the algorithm converges and stops; otherwise, the penalty parameters and exchanged prices are adaptively updated, and the process repeats from the fourth step.

5. Simulation results

In this study, the simulation framework begins with the cleared schedules of the day-ahead energy market, which are taken as the baseline input. To reflect forecast uncertainty, Gaussian white noise is applied to load demand and renewable generation profiles, thereby creating production-consumption imbalances. These imbalances trigger

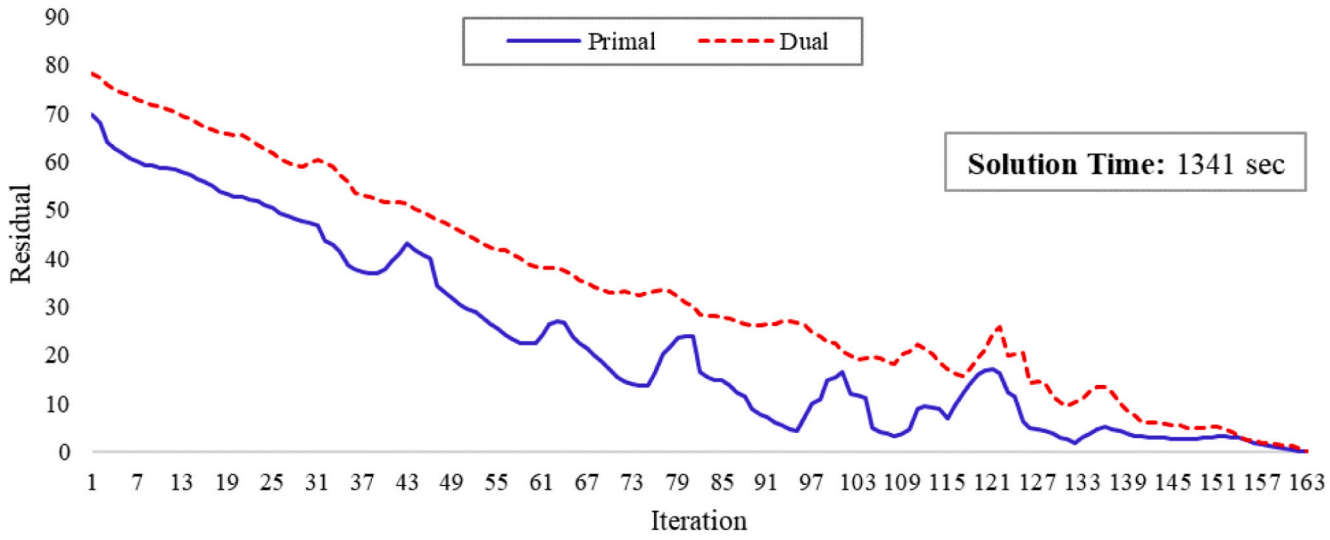

(a) Proposed Adaptive ADMM (C4)

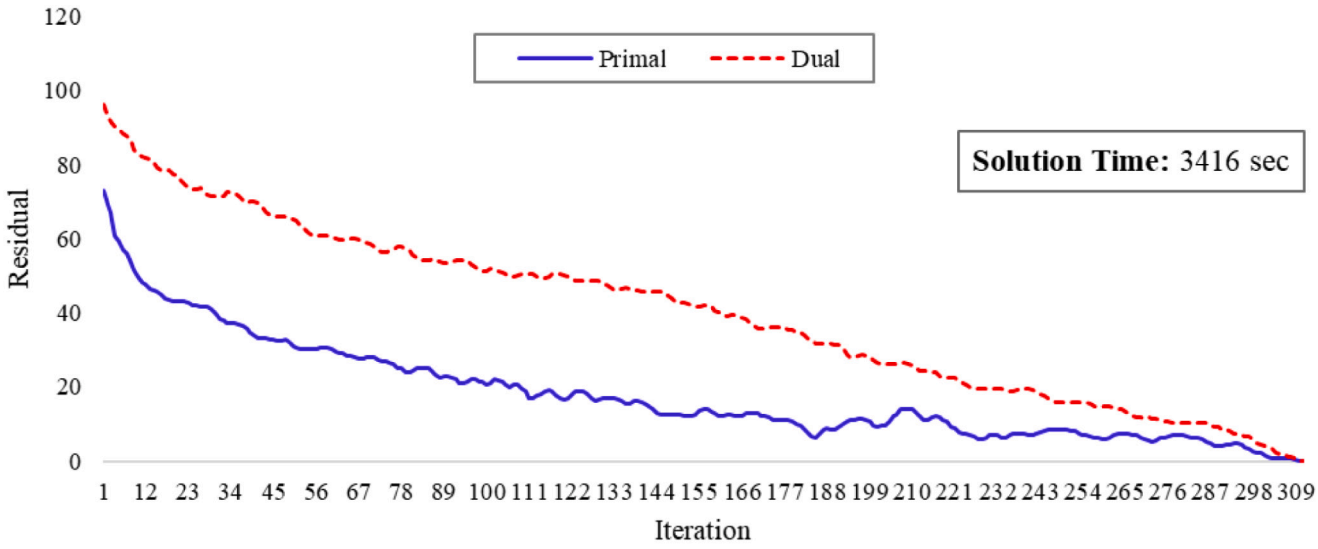

(b) Original ADMM (C5)

Fig. 14. Convergence process of original and proposed adaptive ADMM algorithms.

the intraday flexibility market, where the proposed bi-level model coordinates demand-side resources and storage systems to restore balance. The case study is conducted on the modified IEEE 30-bus test system [38], whose structure is illustrated in Fig. 3. This model has been tested in five different case studies, the details of which are presented in Table 1. These case studies are designed to evaluate the effects of unlocking the flexible capacities of demand-side resources and storage systems on the technical and economic indicators of the system in the balancing market, as well as to assess the accuracy and speed of convergence of the proposed adaptive ADMM. Fig. 4a–f depicts parameters related to load demand, wind speed, and solar radiation in both the DA energy and intra-day balancing markets. Parameters related to the DA energy market are provided with an hourly step, while those of the intra-day balancing market are provided with a 15-minute step. To generate parameters for the balancing market, the energy market parameters are first converted into 96 steps using interpolation, and then white noise is applied to them using the Gaussian distribution function to create unbalancing production-consumption conditions in the system. The load demand curves of FLs and EV parking lots before participating in the balancing market are shown in Fig. 5a and b, respectively. Table 2 provides information on the location and capacity of generation units, storage systems under VSP control, FLs, and EV parking lots.

Table 3 represents the numerical results obtained from C1–C5. In C1, the only providers of balancing services are the dispatchable units of the transmission network, while in C2, the VSP is also activated as a provider of balancing services in the market. According to the results in Table 3, the activation of the VSP in the balancing market has led to a 6.7 % reduction in daily TSO costs, which highlights the direct economic benefit of mobilizing aggregated storage resources.

Fig. 6a–d depicts the resulting schedules for the storage systems under VSP control. Examination of these schedules reveals that the charging and discharging of BSSs, CAESs, and PHESs are in complete

alignment with TSO balancing requirements. Specifically, these units absorb electricity during periods of downward balancing requirements and discharge electricity during periods of upward balancing requirements. This behavior reflects the fundamental physical mechanism of energy storage systems in balancing supply and demand: they act as energy buffers that shift consumption and injection across time, thereby reducing the need for expensive redispatch of conventional thermal units and improving the overall cost-effectiveness of system operation. Fig. 6d provides further insight into the operational dynamics of PHES by illustrating the water levels in the upper and lower reservoirs. As shown, during downward balancing periods, PHES utilizes electricity to pump water from the lower to the upper reservoir. Conversely, during upward balancing periods, the stored water is released back down to the lower reservoir through turbines, generating electricity and supporting the TSO in covering peak upward balancing demand. This cycle demonstrates how PHES enables the storage of surplus renewable energy and its later deployment when demand rises, directly contributing to grid reliability, reducing curtailment of renewables, and providing inertia-like support to the system.

Fig. 7a and b illustrates the balancing service providers in C1 and C2. Fig. 7a shows that the dispatchable units alone provided all the required balancing capacities for the TSO in C1, resulting in higher costs and greater reliance on thermal resources. Conversely, Fig. 7b demonstrates that the activation of the VSP in the balancing market in C2 redistributes part of the balancing provision to storage systems. Among these, PHES contributes the most, owing to its large capacity and flexibility in both pumping and generation modes. This redistribution has important engineering implications: it indicates that deploying storage as a coordinated portfolio under the VSP reduces dependence on thermal generation, substitutes expensive peaking resources with cost-effective flexibility, and increases the robustness of the system to renewable variability.

Finally, Fig. 8 compares the voltage profile at 21:45 in C1 and C2, which corresponds to the time with the highest upward balancing demand. The results show that the activation of the VSP in C2 improves the system's voltage profile, particularly at buses connected to the storage systems. This improvement is not only a numerical outcome but also reflects a physical mechanism: when storage discharges during upward balancing, it injects active power locally, which helps maintain bus voltages and reduces stress on remote transmission lines. The engineering implication is that distributed storage, when coordinated through a VSP, can enhance local voltage stability, alleviate congestion, and improve system resilience under high renewable penetration.

In C3, FLs are incorporated into the pool of balancing service providers. The numerical data in Table 3 indicate that the participation of FLs decreases the TSO's daily balancing costs by 12.2 % compared to C1 and by 5.8 % compared to C2. This reduction confirms that demand-side flexibility can replace part of the expensive balancing capacity traditionally provided by dispatchable units. Fig. 9a–h shows the load demand curves of FLs before and after their engagement in the balancing market. These figures demonstrate the essential mechanism by which FLs contribute: when the TSO requires upward balancing services, the FLs reduce their load consumption, and when downward balancing services are required, they increase consumption. This bidirectional adjustment provides a dual benefit. On the one hand, it enables the TSO to meet balancing requirements at lower cost through distributed and responsive loads. On the other hand, it creates financial opportunities for FL owners by allowing them to monetize their flexibility. The engineering implication is that flexible demand not only substitutes for conventional generation in providing balancing but also strengthens system resilience by absorbing variability where it physically occurs in the network.

Fig. 10a and b compares the share of balancing service providers in C2 and C3. The results reveal that the activation of FLs reduces the dependence on dispatchable units. Among the FLs, industrial loads located at buses 7, 8, and 9 capture a larger market share than residential loads, reflecting their greater ability to shift or curtail demand. In the model, residential FLs are assumed to adjust consumption by up to 12 %, while industrial FLs can vary demand by up to 20 %, either increasing or decreasing depending on the balancing signal. This difference in capability reflects real-world physical constraints: industrial loads typically have more controllable processes and larger baseline demands, while residential loads are limited by consumer comfort and lifestyle requirements. These results underline the importance of recognizing heterogeneity among FLs when designing market mechanisms.

In C4, EV parking lots are introduced as additional providers of balancing services. The data in Table 3 show that their participation reduces TSO's daily balancing costs by 7.4 % compared to C3. This reduction results from substituting part of the capacity of costly dispatchable units with the more affordable flexibility of EV parking lots. Fig. 11a–f depicts the schedules of parking lots after participating in the balancing market. These figures highlight that EV parking lots adjust their initial charging/discharging patterns in direct response to TSO balancing signals. Specifically, during upward balancing periods, the parking lots discharge stored energy from EV batteries into the grid, while during downward balancing periods, the EVs are switched to charging mode to absorb excess electricity. This response reflects the intrinsic physical mechanism of EV batteries as distributed storage assets: they can rapidly alter their charging state to provide short-term balancing capacity.

It is important to note, however, that the operation of EV parking lots is bounded by practical constraints, including the expected departure times of vehicles and the requirement that batteries maintain sufficient charge for users at departure. These factors reduce the absolute flexibility available, yet the results confirm that EV parking lots can still deliver meaningful balancing services within these constraints. Fig. 12a and b compares the composition of balancing capacities in C3 and C4, clearly showing that the inclusion of EV parking lots further reduces the reliance on dispatchable units. Moreover, the EV parking lots achieve a direct financial return of $270.48, illustrating the potential of this resource to generate revenue streams while contributing to system-level cost reductions.

Fig. 13a and b compares the voltage profiles and transmission losses between C4 and C1 to assess the broader technical impacts of simultaneous participation of demand-side resources and VSP-controlled storage. Fig. 13a shows a notable improvement in the voltage profile, especially at buses directly connected to these resources. This improvement is a result of the localized injection or absorption of power, which reduces stress on the transmission system and mitigates voltage drops at critical nodes. Fig. 13b indicates that system losses decrease in C4 compared to C1, especially when demand-side and storage resources contribute significant amounts of balancing power.

Finally, Fig. 14a and b compares the convergence processes of the proposed adaptive ADMM and the original version. Both reach the global optimum, but the adaptive ADMM achieves convergence in 146 fewer iterations, corresponding to a 60 % reduction in solution time. The advantage stems from the adaptive updating of penalty coefficients per coupling interface, which accelerates the reconciliation between TSO and service providers at each iteration. The engineering implication is significant: faster convergence is crucial for intraday and near-real-time markets, where decisions must be taken within limited time windows. Thus, the adaptive ADMM not only ensures theoretical optimality but also enhances the practical applicability of the framework in real-world market environments.

6. Conclusion

This paper presents a bi-level structure designed to harness the potential of demand-side resources and grid-connected storage systems in the flexibility market of renewable-based power systems. At the upper level, the TSO is modeled, while at the lower level, balancing service

providers, including FLs, EV parking lots, and VSP, are modeled. The proposed model enables the VSP to execute charge/discharge planning for the grid-connected storage systems, including BESs, CAESs, and PHESs, in response to flexibility requests from the TSO. To ensure convergence of the upper and lower levels within a decentralized optimization space with minimal information sharing, an adaptive version of the ADMM algorithm has been introduced. The proposed model is implemented using the GUROBI solver in GAMS on a 30-bus transmission system. The highlights of its achievements are as follows:

- The adaptive ADMM version not only meets the market efficiency standard while ensuring limited information sharing but also achieves convergence of the upper and lower levels with 146 fewer iterations than the original version of the algorithm, saving 60 % in solving time.
- The proposed structure effectively unlocks all available flexible capacities on the demand side, including those provided by FLs and EV parking lots in the balancing market. In addition to ensuring their market profitability, the structure reduces system balancing costs by 12.8 %. This cost reduction results from substituting expensive flexible capacities of dispatchable units with the more affordable capacities offered by FLs and EV parking lots. The results also highlight that the deployment of demand-side capacities in the flexibility market reduces transmission losses by about 12 % and enhances voltage profile.
- The proposed bi-level model enables the VSP to operate various storage systems, including BESs, CAESs, and PHESs, in perfect alignment with the TSO's balancing needs, significantly contributing to the provision of flexible capacities. This mechanism not only ensures profitability for the VSP but also reduces system balancing costs by 6.7 %.

While the findings highlight the potential of the proposed framework, several limitations should be acknowledged. First, the use of a linearized power flow introduces approximation errors compared to a full AC formulation, which may affect the accuracy of results in heavily loaded or highly meshed networks. Second, although our mechanism minimizes the amount of information exchanged between the TSO and service providers, we have not introduced a formalized privacy metric to quantify confidentiality levels. These limitations point to future research directions. Extending the approach to non-convex AC-power flow formulations would improve modeling fidelity and enable testing in more realistic operating conditions. Developing and integrating privacy-preserving techniques, such as differential privacy or secure multi-party computation, could provide stronger confidentiality guarantees while maintaining efficiency. Finally, testing the framework on larger-scale systems with real operational data would further validate its scalability and practical relevance.

CRediT authorship contribution statement

Saeid Fatemi: Writing – original draft, Visualization, Software, Methodology, Data curation, Conceptualization. **Abbas Ketabi:** Writing – original draft, Validation, Supervision, Project administration, Funding acquisition, Formal analysis. **Seyed Amir Mansouri:** Writing – original draft, Validation, Software, Methodology, Conceptualization.

Declaration of competing interest

The authors declare that they have no known competing financial interests or personal relationships that could have appeared to influence the work reported in this paper.

Acknowledgement

The research is supported by the University of Kashan under postdoctoral grant number 1403/4920.

Data availability

Data will be made available on request.

References

[1] K. Shafiei, A. Seifi, M.T. Hagh, A novel multi-objective optimization approach for resilience enhancement considering integrated energy systems with renewable energy, energy storage, energy sharing, and demand-side management, J Energy Storage 115 (2025) 115966, https://doi.org/10.1016/j.est.2025.115966.
[2] S.A. Mansouri, E. Nematbakhsh, A.R. Jordehi, M. Marzband, M. Tostado-Véliz, F. Jurado, An interval-based nested optimization framework for deriving flexibility from smart buildings and electric vehicle fleets in the TSO-DSO coordination, Appl. Energy 341 (2023) 121062, https://doi.org/10.1016/j.apenergy.2023.121062.
[3] S.A. Mansouri, A. Ramos, J.P.C. Ávila, J. García-González, J.A. Aguado, A DSO-driven privacy-preserving mechanism for managing power exchanges in Australian networks, IEEE Trans. Ind. Inform. (2025) 1–11, https://doi.org/10.1109/TII.2025.3586048.
[4] K. Kusakana, Optimal peer-to-peer energy management between grid-connected prosumers with battery storage and photovoltaic systems, J Energy Storage 32 (2020) 101717, https://doi.org/10.1016/j.est.2020.101717.
[5] L. He, H. Mo, Y. Zhang, L. Wu, J. Tang, Adaptive energy management strategy for Extended Range Electric Vehicles under complex road conditions based on RF-IGWO and MGO algorithms, Energy 328 (2025) 136500, https://doi.org/10.1016/j.energy.2025.136500.
[6] Z. Wu, Y. Feng, X. Li, B. Yuan, Flexibility definition and improvement of pumped hydro storage: A techno-economic analysis, J Energy Storage 93 (2024) 112078, https://doi.org/10.1016/j.est.2024.112078.
[7] K. Cui, C. Wang, Z. Liu, D. Fu, G. Chen, W. Li, et al., Efficiency analysis of ocean compressed air energy storage system under constant volume air storage conditions, Energy 329 (2025) 136531, https://doi.org/10.1016/j.energy.2025.136531.
[8] A. Burgio, D. Cimmino, M. Dolatabadi, M. Jasinski, Z. Leonowicz, P. Siano, Virtual energy storage system for peak shaving and power balancing the generation of a MW photovoltaic plant, J Energy Storage 71 (2023) 108204, https://doi.org/10.1016/j.est.2023.108204.
[9] M. Krpan, X. Wang, M. Beus, A. Parisio, I. Kuzle, Distributed control of a virtual storage plant for frequency restoration services: an experimental validation, Int. J. Electr. Power Energy Syst. 159 (2024) 110031, https://doi.org/10.1016/j.ijepes.2024.110031.
[10] J. Elio, M. Peinado-Guerrero, R. Villalobos, R.J. Milcarek, An energy storage dispatch optimization for demand-side management in industrial facilities, J Energy Storage 53 (2022) 105063, https://doi.org/10.1016/j.est.2022.105063.
[11] I. Mezghani, N. Stevens, A. Papavasiliou, D.I. Chatzigiannis, Hierarchical coordination of transmission and distribution system operations in european balancing markets, IEEE Trans. Power Syst. 38 (2023) 3990–4002, https://doi.org/10.1109/tpwrs.2022.3208968.
[12] G. Mohy-ud-din, K.M. Muttaqi, D. Sutanto, A Cooperative Energy Transaction Model for VPP Integrated Renewable Energy Hubs in Deregulated Electricity Markets, IEEE Trans. Ind. Appl. 58 (2022) 7776–7791, https://doi.org/10.1109/tia.2022.3195965.
[13] S. Potenciano Menci, O. Valarezo, Decoding design characteristics of local flexibility markets for congestion management with a multi-layered taxonomy, Appl. Energy 357 (2024) 122203, https://doi.org/10.1016/j.apenergy.2023.122203.
[14] K. Steriotis, K. Sepetanc, K. Smpoukis, N. Efthymiopoulos, P. Makris, E. Varvarigos, et al., Stacked revenues maximization of distributed battery storage units via emerging flexibility markets, IEEE Trans. Sustainable Energy 13 (2022) 464–478, https://doi.org/10.1109/tste.2021.3117313.
[15] C.P. Barala, P. Mathuria, R. Bhakar, Distribution locational marginal price based hierarchical scheduling framework for grid flexibility from virtual energy storage systems, Electr. Pow. Syst. Res. 214 (2023) 108866, https://doi.org/10.1016/j.epsr.2022.108866.
[16] K. Pandžić, H. Pandžić, I. Kuzle, Virtual storage plant offering strategy in the day-ahead electricity market, Int. J. Electr. Power Energy Syst. 104 (2019) 401–413, https://doi.org/10.1016/j.ijepes.2018.07.006.
[17] K. Ma, J. Yang, P. Liu, Relaying-Assisted Communications for Demand Response in Smart Grid: Cost Modeling, Game Strategies, and Algorithms, IEEE J Sel Areas Commun 38 (2020) 48–60, https://doi.org/10.1109/JSAC.2019.2951972.
[18] G. Li, Z. Luo, C. Liao, Power capacity optimization and long-term planning for a multi-energy complementary base towards carbon neutrality, Energy 334 (2025) 137644, https://doi.org/10.1016/j.energy.2025.137644.
[19] J. Song, N. Wang, Z. Zhang, H. Wu, Y. Ding, Q. Pan, et al., Fuzzy optimal scheduling of hydrogen-integrated energy systems with uncertainties of renewable generation considering hydrogen equipment under multiple conditions, Appl. Energy 393 (2025) 126047, https://doi.org/10.1016/j.apenergy.2025.126047.
[20] J. Feng, Y. Yao, Z. Liu, Developing an optimal building strategy for electric vehicle charging stations: automaker role, Environ. Dev. Sustain. 27 (2025) 12091–12151, https://doi.org/10.1007/s10668-024-05326-6.
[21] Z. Dou, Z. Ye, C. Zhang, H. Liu, Development and process simulation of a biomass driven SOFC-based electricity and ammonia production plant using green hydrogen; AI-based machine learning-assisted tri-objective optimization, Int. J.

Hydrogen Energy 133 (2025) 440–457, https://doi.org/10.1016/j.ijhydene.2025.04.497.
[22] H. Liu, L. Tang, Z. Dou, S. Wang, D. Yu, Optimizing integrated hydrogen liquefaction with LNG cold energy: A thermoeconomic assessment, comparative analysis, and feasibility study with emphasis on composite curves and uncertainty scrutiny, Energy 315 (2025) 134416, https://doi.org/10.1016/j.energy.2025.134416.
[23] Q. Meng, S. Hussain, Y. He, J. Lu, J.M. Guerrero, Multi-timescale stochastic optimization for enhanced dispatching and operational efficiency of electric vehicle photovoltaic charging stations, Int. J. Electr. Power Energy Syst. 172 (2025) 111096, https://doi.org/10.1016/j.ijepes.2025.111096.
[24] B. Zhang, B. Talihati, H. Fan, Y. Sun, Y. Wang, A dynamic carbon flow traceability framework for integrated energy systems, J. Clean. Prod. 518 (2025) 145878, https://doi.org/10.1016/j.jclepro.2025.145878.
[25] Y. Tang, K. He, H. Shu, K. Wang, W. Lou, Z. Qin, et al., Reliability and safety assessment of distribution networks in mountainous plateau areas subject to low-amplitude lightning, Reliab. Eng. Syst. Saf. 264 (2025) 111305, https://doi.org/10.1016/j.ress.2025.111305.
[26] H. Yang, R. Liang, Y. Zheng, S. Peng, A. Rae, E. Ackom, et al., Receding horizon optimization of power demand response for production-oriented users with real-time operating status-awareness, IEEE Trans. Consum. Electron. PP (2025) 1, https://doi.org/10.1109/TCE.2025.3608740.
[27] M. Jiang, Y. Zhang, Y. Zhang, Multi-depot electric bus scheduling considering operational constraint and partial charging: A case study in Shenzhen, China, Sustainability 14 (2022), https://doi.org/10.3390/su14010255.
[28] M. Yang, Y. Guo, Wind power cluster ultra-short-term prediction error correction method based on the load peak and valley characteristics, CSEE J. Power Energy Syst. (2023) 1–12, https://doi.org/10.17775/CSEEJPES.2022.06180.
[29] J.A. Aguado, Á. Paredes, Coordinated and decentralized trading of flexibility products in Inter-DSO Local Electricity Markets via ADMM, Appl. Energy 337 (2023) 120893, https://doi.org/10.1016/j.apenergy.2023.120893.
[30] L. Marques, A. Sanjab, Y. Mou, H.L. Cadre, K. Kessels, Grid impact aware TSO-DSO market models for flexibility procurement: Coordination, pricing efficiency, and information sharing, IEEE Trans. Power Syst. (2022) 1–14, https://doi.org/10.1109/TPWRS.2022.3185460.
[31] K. Zhang, S. Troitzsch, S. Hanif, T. Hamacher, Coordinated market design for peer-to-peer energy trade and ancillary services in distribution grids, IEEE Trans. Smart Grid 11 (2020) 2929–2941, https://doi.org/10.1109/TSG.2020.2966216.
[32] Á. Paredes, J.A. Aguado, P. Rodrí-guez, Uncertainty-aware trading of congestion and imbalance mitigation services for multi-DSO local flexibility markets, IEEE Trans. Sustainable Energy (2023) 1–13, https://doi.org/10.1109/tste.2023.3257405.
[33] C. Gu, J. Wang, L. Wu, Distributed energy resource and energy storage investment for enhancing flexibility under a TSO-DSO coordination framework, IEEE Trans. Autom. Sci. Eng. (2023) 1–13, https://doi.org/10.1109/tase.2023.3272532.
[34] S.A. Mansouri, A. Rezaee Jordehi, M. Marzband, M. Tostado-Véliz, F. Jurado, J. A. Aguado, An IoT-enabled hierarchical decentralized framework for multi-energy microgrids market management in the presence of smart prosumers using a deep learning-based forecaster, Appl. Energy 333 (2023) 120560, https://doi.org/10.1016/j.apenergy.2022.120560.
[35] Z. Topalović, R. Haas, M. Sayer, Economic benefits of PHS and Li-ion storage. Study cases: Austria and Bosnia and Herzegovina, Appl. Energy 362 (2024) 122988, https://doi.org/10.1016/j.apenergy.2024.122988.
[36] L. Migliari, D. Micheletto, D. Cocco, A hydrogen-fuelled compressed air energy storage system for flexibility reinforcement and variable renewable energy integration in grids with high generation curtailment, Energ. Convers. Manage. 306 (2024) 118308, https://doi.org/10.1016/j.enconman.2024.118308.
[37] S.A. Mansouri, E. Nematbakhsh, A. Ramos, M. Tostado-Véliz, J.A. Aguado, J. Aghaei, A robust ADMM-enabled optimization framework for decentralized coordination of microgrids, IEEE Trans. Ind. Inform. 21 (2025) 1479–1488, https://doi.org/10.1109/TII.2024.3478274.
[38] S. Duman, U. Güvenç, Y. Sönmez, N. Yörükeren, Optimal power flow using gravitational search algorithm, Energ. Conver. Manage. 59 (2012) 86–95, https://doi.org/10.1016/j.enconman.2012.02.024.